This is a preprint, the final version is subject to change, of the American Mineralogist (MSA)
Cite as Authors (Year) Title. American Mineralogist, in press.
DOI: https://doi.org/10.2138/am-2020-7256

Revision 1

Micro- and Nano-Size Hydrogarnet Clusters and Proton Ordering in Calcium Silicate Garnet: Part I. The Quest to Understand the Nature of "Water" in Garnet Continues

Charles A. Geiger[*,1] and George R. Rossman[2]

[1] Department of Chemistry and Physics of Materials
Section Materials Science and Mineralogy, Salzburg University
Jakob Haringer Strasse 2a
A-5020 Salzburg, Austria

[2] Division of Geological and Planetary Sciences
California Institute of Technology
Pasadena, CA 91125-2500, USA

*Corresponding author
Tel. (0431) 662-8044-6226
E-mail: ca.geiger@sbg.ac.at

Submitted to American Mineralogist: 12.11.2019

ABSTRACT

The calcium-silicate garnets, grossular - $Ca_3Al_2Si_3O_{12}$, andradite - $Ca_3Fe^{3+}{}_2Si_3O_{12}$ and their solid solutions $Ca_3(Al_x,Fe^{3+}{}_{1-x})_2Si_3O_{12}$, can incorporate various amounts of structural OH^-. This has important mineralogical, petrological, rheological and geochemical consequences and extensive experimental investigations have focused on the nature of "water" in these phases. However, it was not fully understood how OH^- was incorporated and this has seriously hampered the interpretation of different research results. IR single-crystal spectra of a number of nominally anhydrous calcium silicate garnets, both "end-member" and solid-solution compositions, were recorded at room temperature and 80 K between 3000 and 4000 cm^{-1}. Five synthetic hydrogarnets in the system $Ca_3Al_2(SiO_4)_3$-$Ca_3Al_2(H_4O_4)_3$-$Ca_3Fe^{3+}{}_2(SiO_4)_3$-$Ca_3Fe^{3+}{}_2(H_4O_4)_3$ were also measured via IR ATR powder methods. The various spectra are rich in complexity and show a number of OH^- stretching modes at wavenumbers between 3500 and 3700 cm^{-1}. The data, together with published results, were analyzed and modes assigned by introducing atomic-vibrational and crystal-chemical models to explain the energy of the OH^- dipole and the structural incorporation mechanism of OH^-, respectively. It is argued that OH^- is located in various local microscopic- and nano-size $Ca_3Al_2H_{12}O_{12}$- and $Ca_3Fe^{3+}{}_2H_{12}O_{12}$-like clusters. The basic substitution mechanism is the hydrogarnet one, where $(H_4O_4)^{4-} \Leftrightarrow (SiO_4)^{4-}$, and various local configurations containing different numbers of $(H_4O_4)^{4-}$ groups define the cluster type. Some spectra also possibly indicate the presence of tiny hydrous inclusion phases, as revealed by OH^- modes above about 3670 cm^{-1}. They were not recognized in earlier studies. Published proposals invoking different hypothetical "defect" and coupled-substitution mechanisms involving H^+ are not needed to interpret the IR spectra, at least for OH^- modes above about 3560 cm^{-1}. Significant mineralogical, petrological, and geochemical consequences result from the analysis and are discussed in the accompanying Part II (this volume) of the investigation.

Key words: Grossular, andradite, nominally anhydrous minerals, H_2O, hydrogarnet clusters, nano scale, IR spectroscopy

INTRODUCTION

Garnet Crystal Chemistry and "Water-rich" Hydrogarnet

Garnet is a remarkable phase for a number of reasons (Geiger 2013). One of them is its ability to adapt its crystal structure to accommodate radically different compositions. Indeed, garnet, as both a synthetic phase and as a mineral, exhibits vast chemical variability. One interesting system is the loosely termed "hydrogarnets" or "water"-bearing garnets. The general crystal-chemical formula of anhydrous or "water-free" garnet is $\{X_3\}[Y_2](Z_3)O_{12}$, where dodecahedral {X}, octahedral [Y], and tetrahedral (Z) represent the three special crystallographic cation sites and their polyhedral coordination in space group $Ia\bar{3}d$. In most rock-forming garnets $Z = Si^{4+}$. In true "hydrogarnet", however, the crystallographically single Z cation is absent and, instead, it is replaced and charge balanced locally by four protons. The resulting general crystal-chemical formula can be written as $\{X_3\}[Y_2](H_{12})O_{12}$ or $\{X_3\}[Y_2](H_4O_4)_3$. The former expression is more suitable for describing the vibrational behavior of hydrogarnet and the latter the static crystal chemistry (see discussion below).

Cornu (1905; 1906) was the first to discover hydrogarnet, which he termed hibschite. Other reports of hydrogarnet followed (e.g., Foshag 1920; Belyankin and Petrov 1939; Belyankin and Petrov 1941a) and Foshag introduced the name plazolite for his specimen. Belyankin and Petrov (1941a; 1941b), in their studies, offered the first simplified and correct formula for hibschite as $3CaO{\cdot}Al_2O_3{\cdot}2SiO_2{\cdot}2H_2O$. Passaglia and Rinaldi (1984) analyzed the situation and proposed that the term katoite should be reserved for $Ca_3Al_2(SiO_4)_3$-$Ca_3Al_2(H_4O_4)_3$ garnets with more than 50 mol % of the latter component and hibschite for those with less than 50%. These two workers, as well as Ferro et al. (2003), described new katoite localities and investigated the garnet crystal structures.

It may well have been that Thorvaldson and Grace (1929) and Thorvaldson et al. (1929) were the first to synthesize and characterize $Ca_3Al_2(H_4O_4)_3$. It can be easily synthesized by reacting $Ca_3Al_2O_6$ with water at 1 atm. The reaction is highly exothermic and it is important in the

crystallization sequence of some cements including portlandite. Flint et al. (1941) showed that there can be complete solid solution between $Ca_3Al_2(H_4O_4)_3$ and $Ca_3Al_2(SiO_4)_3$ (see also Flint and Wells 1941; Carlson 1956; Kobayashi and Shoji 1983; Dilnesa et al. 2014). The exchange $(H_4O_4)^{4-} \Leftrightarrow (SiO_4)^{4-}$ or $(4H)^{+} \Leftrightarrow (Si)^{4+}$ was, thus, indicated. Crystal structure determinations of synthetic $Ca_3Al_2(H_4O_4)_3$ using diffraction experiments proved this (Cohen-Addad et al. 1967; Foreman 1968; Lager et al. 1987). Such complete exchange between four protons and a single Si^{+} cation in a silicate is unique in the mineralogical kingdom, as best we know. More recent synthesis results have proposed that the degree of solid solution is temperature dependent and that a miscibility gap can exist along the $Ca_3Al_2(H_4O_4)_3$-$Ca_3Al_2(SiO_4)_3$ join (Jappy and Glasser 1991/92). Water-rich hydrogrossular occurs in relatively low-temperature geologic environments consistent with its *P-T* phase stability (Flint et al. 1941; Carlson 1956; Dilnesa et al. 2014). Yoder (1950) investigated the high *P-T* phase relations of grossular under dry and hydrothermal conditions and discussed the stability of $Ca_3Al_2(SiO_4)_3$ and $Ca_3Al_2(H_4O_4)_3$ solid solutions. His study was extended by Pistorius and Kennedy (1960) in their experimental high *P-T* investigation of grossular and hydrogrossular.

Other hydrogarnets, both end-member and solid-solution compositions, have been prepared in the laboratory (e.g., Ito and Frodel 1967; Albrecht et al. 2019), but none of them have been found in nature. The binary andradite ($Ca_3Al_2(SiO_4)_3$)-"hydroandradite" ($Ca_3Al_2(H_4O_4)_3$) has been demonstrated by laboratory synthesis experiments to show an extensive degree of substitutional solid solution (Flint et al. 1941; Dilnesa et al. 2014). The precise phase relations are difficult to determine because of kinetic issues. The synthesis of end-member $Ca_3Fe^{3+}{}_2H_{12}O_{12}$ has apparently not yet been fully achieved (e.g. Kuzel 1968) and its thermodynamic stability appears to be restricted to below roughly 60 °C (Lothenbach pers. comm.). Kresten et al. (1982) reported the occurrence of a hydroandradite from Sweden and Armbruster (1995) refined the crystal structure a hydrous andradite from South Africa.

"Water" in nominally anhydrous silicate garnet

An initial report (Wilkins and Sabine 1973) of various rock-forming silicates containing small concentrations of H_2O, including garnet, was largely ignored for years and probably was viewed as a "mineralogical curiosity" by the broader community. However, following reports of the presence of OH^- in different rock-forming garnet species (e.g., Beran et al. 1983; Aines and Rossman 1984), which, moreover, could be measured straightforwardly with IR single-crystal methods, research in this area intensified. Study has been directed at number of other so-called "NAMs", which is short for nominally anhydrous minerals. Interest increased greatly and scientists began discussing, for example, how many "oceans of water" could be contained in Earth's upper mantle (Bell and Rossman 1992) and the geochemical and geophysical ramifications. Important mineral groups like olivine, pyroxene, and feldspar, for example, were studied in various ways and in terms of their minor water contents (see reviews of Ingrin and Skogby 2000 and Peslier 2010). The state of research on NAMs is now rather mature.

To determine the presence of OH^- in garnet, or any other nominally anhydrous mineral for that matter, IR spectroscopy has been the method of choice. Legions of single-crystal IR spectra (and some Raman spectra as well) have been recorded on various garnet species and compositions, both natural and synthetic. They show a plethora of different energy vibrational OH^- stretching modes. However, in spite of the great amount of study, conclusive assignments of the protons to exact structural sites in the crystals have remained elusive. The nature of these minor concentration OH^- groups in garnet is not well understood in a crystal-chemical sense, with a few exceptions (see Geiger and Rossman 2018). It is not understood if the OH^- groups are just some ill-defined defect(s) or whether they occupy more than one crystallographic position in an ordered manner (e.g., Basso et al. 1984; Basso and Cabella 1990). Or does their presence represent some atomic-coupled-substitution mechanism, for example, $(Al^{3+}\text{-}H^{+})^{4+} = (Si^{4+})$ or are they linked to "nonstandard garnet" elements $\{Li^{+}\text{-}H^{+}\} = \{Ca,Mg,Fe^{2+},Mn^{2+}\}$ - see references and discussion in Part II (Geiger and Rossman this volume)? Most astonishingly, considering the degree of study and the "stage of the game", it is not known how structural OH^- is incorporated in most natural

garnets (e.g., as $(H_4O_4)^{4-}$ groups or not). Proton NMR study of synthetic katoite and three natural grossulars showed, depending on the exact garnet in question, the presence of four H-atom clusters (hydrogarnet) and/or two H-atom clusters (Cho and Rossman 1993).

Present thinking or the "ruling scientific mindset" considers that, because the IR spectra of nearly all natural silicate garnets do not match the IR spectra of their synthetic analogues, both in terms of the number of OH^- modes as well as their energies, the two types of crystals must have different OH^- substitutional mechanisms. With regards to the common silicate garnets, a match in IR spectra has only been found between synthetic and natural andradite (Geiger and Rossman 2018). However, the "ruling scientific mindset" that has operated over, say, the past three decades may be wrong. Radical new insight is needed in order to move beyond what has been observed, analyzed and proposed over the last three decades in terms of OH^- in garnet.

Both this investigation and that in Part II (Geiger and Rossman this volume) attempts to do this. The long quest to understand the nature of "water" garnet, and researching the possible occurrence of the hydrogarnet substitution in natural garnets, continues. In order to do this, we studied the OH^- substitution in the four component system $Ca_3Al_2(SiO_4)_3$-$Ca_3Al_2(H_4O_4)_3$-$Ca_3Fe^{3+}_2(SiO_4)_3$-$Ca_3Fe^{3+}_2(H_4O_4)_3$ by examining both synthetic and natural garnets. The main experimental input is from IR spectroscopy. An analysis of the results is undertaken that is based on the atomic-vibrational and crystal-chemical properties of calcium silicate garnets.

SAMPLES USED FOR STUDY AND EXPERIMENTAL METHODS

The garnets measured via IR single-crystal and powder ATR spectroscopy are from the personal collections of CAG and GRR. The various samples are described in Table 1. Many of the single crystals have been characterized via microprobe analysis and studied in some form before, including by IR spectroscopy in the energy range between 3000 and 4000 cm^{-1}. For example, the large collection of grossular spectra of Rossman and Aines (1991) were measured with a grating spectrometer, whereas other spectra shown herein were measured with various Fourier-transform

IR spectrometers. Newer and better spectrometers allow more spectral detail to be revealed. Moreover, several garnet crystals were measured at low temperatures ultimately down to 80 K. The experimental set-up in terms of the more recent measurements has been described before (e.g., Geiger and Rossman 2018).

Infrared spectra of synthetic hydrogarnet powders (courtesy of B. Lothenbach to CAG) were obtained on a Nicolet iS50 FTIR spectrometer with the ATR method using a SensIR Technologies DuraScope diamond ATR accessory. Before each measurement, the diamond crystal was cleaned with ethanol and the diamond surface was fully covered with sample powder that was pressed against the diamond with a rod that was terminated in aluminum foil. All spectra were corrected with a built in ATR correction that compensated for the penetration depth of the IR radiation into the sample as a function of wavelength.

Spectral results were curve fit using the WiRE program of Renishaw that is part of their Raman systems. Spectra with sloping baselines were first manually baseline-corrected using WiRE.

RESULTS

IR spectra (Figs. 3 and 5 to 12) from our latest measurements, as well as some taken from the literature, will be shown in the course of the discussion (see also Part II – Geiger and Rossman this volume, where, for example, H_2O contents of various water-poor nominally anhydrous garnets are given and discussed). Several words regarding OH^- mode wavenumbers are in order. Because different IR spectrometers with differing experimental set-ups were used to measure the spectra of the various garnets analyzed here, there can be slight a variation in the wavenumber for a certain mode. In addition, the curve fits of a spectrum give the peak center wavenumber, whereas other spectra give the wavenumber at the peak maximum. Fit results also may depend slightly on several factors such as the nature of the baseline correction and band overlap, for example. All these

factors lead to slight variations in the precise wavenumber for a given OH^- mode. We think, in general, that the uncertainty is better than ± 2 cm^{-1} and possibly in some cases within ± 1 cm^{-1}.

We note, further, that our spectral fits are subjective to a certain degree. The issue is complex, in detail, because some spectra contain a fairly large number of modes and band overlap is present. Moreover, there can be considerable differences in band intensities.

DISCUSSION

An understanding of the IR spectra of most natural, water-bearing nominally anhydrous "end-member" garnet species, and especially intermediate solid-solution compositions, in terms of assigning observed OH^- stretching modes, is not at hand (we use quotation marks around the term end-member, because the presence of any amount of OH^- must cause deviations from exact garnet stoichiometry and also because most natural garnets are never compositionally "pure" and stoichiometric).

At this point, with respect to silicate garnets, only certain "end-member" andradite crystals are understood in terms of their OH^- incorporation at least at the first level. It represents the simplest IR spectroscopic case and both natural and synthetic crystals can apparently contain a hydroandradite component, $Ca_3Fe^{3+}{}_2H_{12}O_{12}$ (Geiger and Rossman 2018) via the presence of local and isolated $(H_4O_4)^{4-}$ groups. The vibrational spectrum of synthetic $Ca_3Al_2H_{12}O_{12}$ is also - at least down to about 80 K - well described and understood (Kolesov and Geiger 2005). Our analysis in this study builds upon the conclusions of our earlier work, which proposed criteria to identify the hydrogarnet substitution in terms of IR and Raman spectra and primarily in anhydrous nominally end-member garnets.

We concentrate our efforts in this Part I on the four component system shown in Fig. 1, where the currently accepted garnet terminology is taken from Grew et al. (2013). The IR spectra of these garnets are rich and complex in terms of the number of different energy OH^- bands (or "band patterns") that they exhibit (e.g., Rossman and Aines 1986; Rossman and Aines 1991;

Armbruster and Geiger 1993; Amthauer and Rossman 1998; Withers et al. 1998; Maldener et al. 2003; Kurka et al. 2005; Phichaikamjornwut et al. 2012; Dachs et al. 2012; Dilnesa et al 2014; Reynes et al. 2018). However, the observed OH^- bands have not been assigned and relatively little is understood in terms of the detailed vibrational and crystal-chemical behavior. Before an analysis of the IR results can begin, it is first necessary to describe the crystal chemistry of garnet and understand what vibrational spectra of crystals measure.

Garnet crystal chemistry, general OH^--stretching mode behavior, and stability of the hydrogarnet substitution

Vibrational spectroscopy, here IR and Raman, measures local vibrations of atoms and atomic groups in molecules and crystals (Nakamoto 2009). The IR and Raman spectra of different garnet species and intermediate composition solid solutions in the energy region of the lattice vibrations (1200 to 100 cm^{-1}) have been measured and analyzed based on their crystal chemistry (e.g., Moore et al. 1971; Hofmeister and Chopelas 1991; McAloon and Hofmeister 1993; Kolesov and Geiger 1998; Geiger 1998). The crystal-structure properties of garnet have been investigated and described many times and in great detail, as made possible by a multitude of diffraction studies (e.g., Novak and Gibbs 1971; Armbruster and Geiger 1993; Geiger and Armbruster 1997).

Consider the local crystal chemistry around the crystallographic Wyckoff 24*d* position, space group *Ia*-3*d*, and the cation-oxygen bonding arrangement. The (Z) cation at 24*d,* site symmetry -4, is Si^{4+} for most natural garnets. In garnet containing a hydrogarnet component a Si^{4+} atom is absent and proxied locally by four H^+ (or D^+) atoms, as shown by several neutron diffraction investigations (Cohen-Addad et al. 1967; Foreman 1968; Lager et al. 1987; Lager and Dreele 1996). The protons bisect and lie slightly above the four surfaces of a tetrahedron that is defined by four oxygen atoms to which they are bonded with an OH^- bond length of 0.906(2)/0.925(12) Å (Lager and Dreele 1996). The crystallographic positions of the four H^+ cations result from the atomic forces acting in the garnet and the necessity to maintain *local*

charge balance in the vicinity of the 24*d* site. Crystallographically, there is just a single O atom located at a general position (x,y,z) in garnet. *Thus, there are just single OH^- groups that vibrate and there are no $(H_4O_4)^{4-}$-type vibrations. There are only individual OH^--stretching vibrations in the energy region around 3600 cm^{-1} ± 100 cm^{-1}* (Kolesov and Geiger 2005; Orlando et al. 2006). There is little reason to consider $(H_4O_4)^{4-}$-cluster-like vibrations (i.e., Harmon et al. 1982), because they should not exist. This is a good reason to express the general formula of hydrogarnets as $\{X_3\}[Y_2](H_{12})O_{12}$. Furthermore, it has been argued that there is very weak, if any hydrogen bonding present (Orlando et al. 2006; Geiger and Rossman 2018; cf. Harmon et al. 1982). Thus, this potential complication to OH^- vibrational behavior can probably be ignored, based on the existing results.

The relevant local atomic configuration is shown in Fig. 2. The H^+ atom is bonded to a single oxygen atom that is also chemically bonded to a single Y-cation (Wyckoff 16*a* position) and two X-cations (Wyckoff 24*c* position) with different X-O chemical bond lengths. Because of this arrangement, there must be OH^--mode coupling and/or mixing with Y- and X-cation-related vibrations. For the common silicate garnets, X can be Ca, Mg, Fe^{2+} and Mn^{2+} and Y can be Al^{3+}, Fe^{3+} and Cr^{3+} and they can exchange with one another to various degrees at the X- and Y-sites, respectively, giving a range of compositionally complex substitutional solid solutions (Geiger 2008). There are considerable differences in ionic radii, masses and electronic states among these various cations and, therefore, the associated chemical bonds must be different in nature. Adopting a harmonic oscillator to describe the vibration of an atom pair (A and B), the frequency is given by:

$$\nu = \frac{1}{2\pi}\sqrt{\frac{k}{\mu}} \quad (1),$$

where *k* is the force constant (i.e., in simple terms the bond strength) and μ_{AB} is the reduced mass of the system ($\mu_{AB} = \frac{m_A m_B}{m_A + m_B}$). It is obvious that an O-H stretching mode will have a different vibrational frequency depending on the precise local atomic configuration and the nature of the

various chemical bonds involving the common oxygen atom (Fig. 2) and also possibly beyond. Geiger and Rossman (2018) discussed the case for various OH^--bearing "end-member" garnet species. They all show a single OH^- stretching mode whose energy is a function of the atomic masses and strengths of the different chemical bonds of the "extended vibrational system". The greater the mass, the lower will be the wavenumber of the OH^- stretching mode, ignoring other factors. This reasoning explains, for example, the lower energy of the OH^- stretching mode in the IR spectra (Albrecht et al. 2019) of the synthetic hydrogarnets $Ca_3Cr^{3+}{}_2H_{12}O_{12}$, $Sr_3Cr^{3+}{}_2H_{12}O_{12}$ and $Ca_3Rh^{3+}{}_2H_{12}O_{12}$ (i.e., 3616, 3625 and 3592 cm^{-1}, respectively) compared to that for $Ca_3Al_2H_{12}O_{12}$ (i.e., 3662 cm^{-1}). The OH^- stretching mode observed in RT spectra is generally broad in OH^--bearing garnets because of the large vibrational amplitudes of the H^+ atom (Lager et al. 1987). Cooling the crystal dampens significantly the amplitudes of vibration and the single OH^- band at RT narrows greatly and ultimately at about 80 K or slightly below two modes are observable in IR spectra (Kolesov and Geiger 2005; Geiger and Rossman 2018).

Of course, pure end-member composition silicate garnets are rare, if they even exist in nature. There is almost always some degree of solid solution at the X- and Y-sites. This means there can be various local cation configurations around a given oxygen atom in a solid-solution crystal (Fig. 2). Their concentration depends on the garnet bulk composition. The precise local crystal-chemical situation (i.e., atomic order-disorder and structural relaxation) is complex and it is not fully understood at this time. Suffice it to say, here, that the intensities of the different OH^- stretching modes will depend on the relative amounts of the various local cation configurations. Different vibrational possibilities could exist in a solid-solution garnet. One is that each local atomic configuration will result in a representative OH^- mode with its characteristic energy, as in the respective end-member garnets grossular, andradite or katoite, for example. Another possible behavior is that a distribution of relatively closely spaced OH^- modes, each with not too different energies, occurs. This latter situation can give rise to OH^--band broadening and varying the temperature of the IR measurement will not significantly affect OH^- band widths. This effect is

called chemical-mode broadening in comparison to pure vibrational-mode broadening. In terms of many natural OH^--bearing garnets both can occur.

Finally, it must be stressed, as a key basis for our analysis that the substitution $(H_4O_4)^{4-} \Leftrightarrow (SiO_4)^{4-}$ or $(H_4)^{4+} \Leftrightarrow (Si)^{4+}$ is energetically favorable for grossular-katoite crystals, as shown by synthesis experiments (Flint et al. 1941; Carlson 1956; Kobayashi and Shoji 1983) and also to a large, but not complete, degree in $Ca_3Fe^{3+}{}_2(SiO_4)_3$-$Ca_3Fe^{3+}{}_2(H_4O_4)_3$ garnets (Flint et al. 1941; Dilnesa et al. 2014). No other common silicate binary garnet system shows such complete exchange. Phase equilibrium studies on $Ca_3Al_2(SiO_4)_3$-$Ca_3Al_2(H_4O_4)_3$ solid solutions at high *P* and *T* under hydrothermal conditions indicate that thermal stability increases with decreasing H_2O in the garnet (Yoder 1950; Pistorius and Kennedy 1960). Finally, empirical pair potential calculations show that the reaction grossular + water $\rightarrow$ katoite is thermodynamically favored (Wright et al. 1994).

A simple question is then: why are the IR spectra of nominally anhydrous grossular and other calcium silicate garnets so variable and complex compared to those of other natural silicate garnets (e.g., pyrope, almandine, spessartine) in terms of their OH^- incorporation?

IR spectra, OH^- stretching modes and their assignment, hydrogarnet domains and clusters

Katoite and water-rich katoite-grossular solid solutions

We start our analysis with synthetic end-member katoite, $Ca_3Al_2H_{12}O_{12}$, with a well-known crystal structure (Cohen-Addad et al. 1967; Foreman 1968; Lager et al. 1987) and IR and Raman spectrum (Kolesov and Geiger 2005). At RT its IR spectrum shows a broad, single asymmetric OH^- stretching mode at 3662 cm^{-1}. It can be fit with two components with energies of about 3681 and 3666 cm^{-1} at about 80 K. At even lower temperatures, both the IR and Raman spectra become complex in the OH^- stretching region with the appearance of many new, weak OH^- modes, but this aspect is not considered further here. The OH^- "doublet" at roughly 80 K is asymmetric, whereby the higher energy OH^- band is considerably more intense than the lower energy one. Geiger and

Rossman (2018) argued that this spectroscopic behavior of OH^--mode splitting characterizes the hydrogarnet substitution in most "end-member" silicate garnets.

Consider now the IR single-crystal spectra of intermediate $Ca_3Al_2Si_3O_{12}$-$Ca_3Al_2H_{12}O_{12}$, both natural and synthetic, garnets (Fig. 3 - replotted from Rossman and Aines 1991) containing major H_2O contents. From these five spectra, it is immediately apparent that the band at about 3660 cm^{-1} does not vary greatly in wavenumber, but it decreases in intensity with increasing number of Si atoms in the formula unit (or grossular component). We conclude, therefore, that this mode must represent the presence of katoite-like domains in the solid-solution composition garnets (a strong OH^- band at 3660 cm^{-1}, as well as a couple of others with high wavenumber, were observed in the IR powder in KBr spectra of a series of synthetic $Ca_3Al_2Si_3O_{12}$-$Ca_3Al_2H_{12}O_{12}$ garnets – Kobayashi and Shoji 1983. However, the quality of the published spectra does not permit a precise analysis). The local crystal-chemical situation is shown in Fig. 4a. It can also be observed in a couple of IR spectra (GRR 1329 and GRR 1358) that there is a strong OH^- band between 3595 cm^{-1} and 3660 cm^{-1} that increases in intensity with increasing grossular component in the solid solution (Fig. 3). Rossman and Aines (1991) wrote in their IR study of grossular garnets, "We assign the band at 3598 cm^{-1}, which is dominant in the silica-rich hydrogrossular samples, to $(O_4H_4)^{4-}$ groups, adjacent to SiO_4 groups." We accept this proposal. The local crystal-chemical situation is illustrated in Fig. 4b and it shows a single, isolated $(H_4O_4)^{4-}$ group imbedded in an anhydrous grossular "matrix". The wavenumber of the associated OH^- mode is about 60 cm^{-1} less than in end-member katoite and could be a function of two effects. The first is related to bond strengths. In end-member grossular the two different Ca-O bond lengths (Fig. 2) are Ca(1)-O(4) = 2.322(1) Å and Ca(2)-O(4) = 2.487(1) Å (Geiger and Armbruster 1997). They are shorter, and thus stronger, than in end-member katoite, where Ca(1)-O(4) = 2.465(2) Å and Ca(2)-O(4) = 2.511(1) Å (Lager et al. 1987). It can be expected that local Ca-O bonds in a water-bearing grossular vary in length depending on the precise structural state within a solid solution. Stronger Ca-O bonds translate to weaker O-H bonds (Geiger and Rossman 2018). Second, it could be

337 expected that there is extended mode coupling and/or mixing beyond the fragment shown in Fig. 2
338 that affects O-H bonding. The presence of heavier Si^{4+} cations compared to H^{+} atoms in a garnet
339 solid solution could act to lower the OH^{-} stretching vibration energy.
340 The IR and Raman spectra indicate, therefore, two "end-member type" H_4O_4 substitution
341 mechanisms. Obvious questions arise however. One is apparent in the spectrum of garnet GRR
342 1058 (Fig. 3). The broad OH^{-} mode envelope has structure and shows a peak maximum at roughly
343 3620 cm^{-1}. How is it to be assigned? More generally, published IR spectra of water-poor grossular
344 show a varying number of OH^{-} bands located between 3660 and 3600 cm^{-1}. How are they to be
345 assigned?
346
347 *"End-member" or nearly end-member grossular*
348 In order to answer this question, we consider the IR spectra of several "end-member" or
349 closely end-member composition grossulars, both synthetic and natural. The spectra of a
350 hydrothermally synthesized grossular (Geiger and Armbruster 1997 - grown from the oxides CaO
351 - from $CaCO_3$, Al_2O_3, and SiO_2) and a nearly end-member composition natural garnet (GRR 53 -
352 Table 1) are shown together in Fig. 5a. The two spectra are remarkably similar in appearance and
353 give the first "spectroscopic match" between a synthetic and a natural crystal (We interject, here,
354 that the IR powder spectra on synthetic grossular recorded by Hsu (1980) show weak absorption
355 features at about 3620 and 3660 cm^{-1} that could be interpreted as indicating structural OH^{-}, as well
356 as a broad and intense absorption band centered at 3420 cm^{-1} that can be assigned to liquid water.
357 It is our experience, though, that IR powder spectra are normally insufficient for characterizing
358 precisely small amounts of OH^{-} in minerals.). The spectra of both the synthetic crystal and GRR
359 53 show three intense OH^{-}-bands at 3666, 3633 and 3623 cm^{-1}. Consider, furthermore, the IR
360 spectra of the synthetic and natural grossulars shown in Fig. 6. They show different OH^{-} spectral
361 features from those garnets in Fig. 5a and have intense modes at 3623 (±1) and 3603 cm^{-1}. The

two garnets give a second spectral "match" between a synthetic and natural end-member composition crystal.

The spectrum of the synthetic grossular in Fig. 5a shows fine structure (e.g., shoulders on the main peaks) indicating the presence of additional OH^- modes and, therefore, it was curve fit to describe them (Fig. 5b). Additional bands at 3688, 3660, 3645, 3613, 3604, 3578, and 3561 cm^{-1} result. This gives a total of ten possible OH^- modes for this synthetic grossular. We analyze and assign them. First, however, we note that the weak modes at 3561, 3579 and 3688 cm^{-1} may be experimental artefacts arising from the difficultly in collecting a spectrum with a smooth baseline on the tiny synthetic crystal. On the other hand, they could also be real and possible assignments are discussed below. Summarizing for the present discussion, here, this gives seven OH^- modes at about 3666, 3660, 3645, 3633, 3623, 3613, and 3604 cm^{-1}. There appears appear to be an approximate regularity in the wavenumber spacing between the modes.

It turns out that these various modes, in various combinations and with differing intensities, are observed in most, if not all, published IR spectra of natural grossular crystals. To be sure, the large number of spectra in Rossman and Aines (1991) show intense OH^- bands at about 3612, 3622, 3633, and 3641 cm^{-1} depending on the specific crystal in question. Indeed, the presence or absence and the intensity of these modes (i.e., the spectral pattern) was used to define or to characterize their different classes of OH^--bearing grossulars. Phichaikamjornwut et al. (2012) in their IR study of different natural grossular-andradite garnets also measured intense modes at about 3602, 3612, 3631, and 3641 cm^{-1}.

All the IR results, analyzed together, indicate a spectral systematics defined by OH^--bands with similar wavenumbers between 3595 and 3670 cm^{-1}. Not every band is present in the spectra of every garnet, but systematic OH^--mode behavior is observable. Thus, we propose that OH^- stretching modes at about 3599, 3612, 3622, 3633, 3641 and 3657 cm^{-1} could arise from the presence of various, local hydrogrossular-like clusters occurring in an anhydrous grossular "matrix". Table 2 lists the different modes (Note: Based on our analysis of many spectra, the mode

388 at about 3657 cm^{-1} appears to be the most problematic in the sense that it often does not occur
389 and/or that it is weak in intensity in the spectra of many garnets. We have no good explanation for
390 this, except to state that this mode is related to a six-membered $(H_4O_4)^-$ cluster - Fig. 4g - that is
391 structurally, and thus probably energetically, similar to a katoite-like cluster - Fig. 4a - having an
392 OH^- mode around 3660 cm^{-1}. Thus, the latter type of cluster may more preferentially occur). From
393 this analysis, seven types of local $(H_4O_4)^{4-}$clusters (and/or domain in the case of water-rich
394 hydrogarnets) can be constructed by having different numbers of $(H_4O_4)^{4-}$ groups in them and they
395 can assigned to the different energy OH^- modes. Fig. 4c-f shows the respective atomic
396 configurations for the different cluster types. According to our model analysis, the OH^- mode
397 wavenumber increases with the number of $(H_4O_4)^{4-}$ groups in a given cluster.
398 Summarizing our analysis, the observed OH^--stretching modes between 3595 and 3670
399 cm^{-1} in the IR spectra for many different OH^--bearing grossulars and katoites can be interpreted
400 and assigned in a completely new context. Figure 7 shows IR spectra including one-water rich
401 grossular and six water-poor samples having an intense OH^- mode at one or more of the
402 characteristic wavenumbers. It must be noted, though, that other OH^- bands can be also observed
403 above and below this wavenumber range (Rossman and Aines 1991; Phichaikamjornwut et al.
404 2012; Dachs et al. 2012; Reynes et al. 2018). This aspect is now considered.
405
406 *Other possible OH^- substitution mechanisms in "end-member" grossular and hydrous inclusions*
407 The IR spectra of water-poor natural grossular can often show OH^- bands that are not listed
408 above and lie at energies above 3670 cm^{-1}. Their assignments are not known and remain to be
409 made. Consider, first, the high-energy OH^- mode at 3684-3688 cm^{-1} at RT that has often been
410 observed (Fig. 8 and see spectra in Rossman and Aines 1991; Kurka et al. 2005; Dachs et al. 2012;
411 Phichaikamjornwut et al. 2012). This mode has stronger O-H bonding compared to those OH^-
412 modes between 3595 and 3662 cm^{-1} and it cannot be assigned based on the model analysis given
413 above. One speculative possibility is that it arises from the substitution $\{2H^+ \Leftrightarrow Ca^{2+}\}$. A H^+ atom,

as part of an OH^- dipole directed towards the interior of an X-cation-free (site 24*d*) oxygen coordinated dodecahedron, should have relatively little interaction with other atoms in the garnet structure. It could be expected to be the "freest OH^- dipole" of any in grossular and thereby have the strongest O-H bond.

Alternatively, this high wavenumber mode might be related to the presence of tiny inclusions of a foreign OH^--bearing phase. High wavenumber OH^- bands (greater than 3670 cm^{-1}) in the spectra of andradite and pyrope have been argued to be due to the presence of inclusions of minute layer silicates such as talc and phlogopite (Geiger et al. 2018; Geiger and Rossman submitted – 2019c). What about grossular? The spectra of serpentine minerals (i.e., chrysotile, lizardite, antigorite) are characterized by OH^- bands with high energies. Schroeder (2002) gives 3686 cm^{-1} for the strong OH^- band for the spectrum of lizardite and Mellini et al. (2002) measured 3684 cm^{-1} for lizardite from Elba Island. Band energies depend on the precise compositions of the phases (Heller-Kallai et al. 1975). The absorption features can be broad in nature and show fine structure and are variable depending on the precise serpentine mineral. A band at about 3674-3677 cm^{-1} can also be observed in some spectra of grossular (Fig. 8). Antigorite can show a strong OH^- band (asymmetric in shape) with a peak maxima of 3674-3678 cm^{-1} (Heller-Kallai et al. 1975; Mellini et al. 2002). Talc, as well, shows an intense OH^- band at 3677 cm^{-1} (Schroeder 2002). It is important to note that nearly end-member grossular crystals can often be found in rhodingites associated with serpentinites (see the discussion in Part II on grossulars from Asbestos, Canada). Therefore, in light of the evidence, the high energy bands at about 3684-3688 and 3674-3677 cm^{-1} in the spectra of grossular are best assigned, at least at this time, to the presence of tiny inclusions of hydrous Mg-rich layer silicates.

In addition to these high wavenumber OH^- modes, other OH^- modes with energies less than about 3595 cm^{-1} have been observed in the spectra of many natural grossulars (Rossman and Aines 1991; Kurka et al. 2005; Phichaikamjornwut et al. 2012; Dachs et al. 2012; this work). We

address them below, but first we consider the IR spectra of synthetic $Ca_3Fe^{3+}{}_2H_{12}O_{12}$-bearing hydrogarnet solid solutions and natural end-member andradite.

Water-rich $Ca_3Fe^{3+}{}_2Si_3O_{12}$-$Ca_3Fe^{3+}{}_2H_{12}O_{12}$-$Ca_3Al_2Si_3O_{12}$-$Ca_3Al_2H_{12}O_{12}$ solid solutions

End-member $Ca_3Fe^{3+}{}_2H_{12}O_{12}$ has yet to be synthesized and, therefore, its OH^- mode energy cannot be measured directly, as was done with $Ca_3Al_2H_{12}O_{12}$. However, water-rich hydrogarnets in the four-component system $Ca_3Fe^{3+}{}_2Si_3O_{12}$-$Ca_3Fe^{3+}{}_2H_{12}O_{12}$-$Ca_3Al_2Si_3O_{12}$-$Ca_3Al_2H_{12}O_{12}$ have been synthesized (Dilnesa et al. (2014). Thus, we made IR ATR powder measurements on five garnets of nominal composition $Ca_3Al_2(Si_{1.0},H_{8.0})O_{12}$, $Ca_3[Al_{1.4},Fe^{3+}{}_{0.6}]_2(Si_{1.0},H_{8.0})O_{12}$, $Ca_3[Al_{1.0},Fe^{3+}{}_{1.0}]_2(Si_{1.0},H_{8.0})O_{12}$, $Ca_3[Al_{0.6},Fe^{3+}{}_{1.4}]_2(Si_{1.0},H_{8.0})O_{12}$, and $Ca_3[Fe^{3+}{}_{2.0}](Si_{0.75},H_{9.0})O_{12}$ (Table 1). The spectra are shown in Fig. 9. Two main absorption features occur at 3611 cm^{-1} and 3658 cm^{-1}. We think these two energies describe the presence of $Ca_3Al_2H_{12}O_{12}$- and $Ca_3Fe^{3+}{}_2H_{12}O_{12}$-like domains in these garnets, respectively. The former mode energy agrees with the spectroscopic results discussed above. Spectral variations as a function of garnet composition are apparent. The OH^- mode (also expressed as a band or a shoulder) at about 3658 cm^{-1} decreases in relative intensity with decreasing $Ca_3Al_2H_{12}O_{12}$ component in the garnet, as expected. Concurrently, the OH^- mode at 3611 cm^{-1} increases in relative intensity with increasing $Ca_3Fe^{3+}{}_2H_{12}O_{12}$ component in the garnet (Fig. 9) - (there also appears to be a weaker OH^- mode at about 3534 cm^{-1} in the spectra of these garnets, but it should have another origin and is not considered in this work).

"End-member" or nearly end-member andradite

The RT IR spectra of a number of "end-member" andradites have been recorded (Amthauer and Rossman 1998; Adamo et al. 2011; Zhang et al. 2015; Geiger et al. 2018). The low-temperature IR spectra of several natural crystals and one synthetic were measured down to 80 K by Geiger and Rossman (2018). The IR spectra of most, but not all, "end-member"

andradites are simpler compared to the situation for grossular in terms of the number of observed OH^- modes. Many spectra of andradite contain just one or two OH^- modes at RT. Most natural and hydrothermally synthesized crystals show the most intense OH^- band, which is broad and asymmetric, at or near 3563 cm^{-1}. It splits into two bands at 3575 cm^{-1} and 3557 cm^{-1} at 80 K (Geiger and Rossman 2018). Or it possibly splits into three modes including the one at 3543 cm^{-1} for andradite GRR 1263 (Fig. 10 and Table 1). At any rate, we consider these bands to represent the presence of single, isolated $(H_4O_4)^{4-}$ groups (Fig. 4b) in andradite (Table 2).

The lower OH^- stretching energy compared to the analogous situation for single, isolated $(H_4O_4)^{4-}$ groups in grossular is largely due to the fact that the mass of Fe^{3+} (55.85 amu) is twice that of Al^{3+} (26.98 amu). Eqn. (1) describes the general situation. The mass effect is clearly demonstrated by the energies of the IR-active translational (T) vibrations of both cations in garnet. The wavenumber range for T(Fe^{3+}) modes lies between 130 and 360 cm^{-1} for andradite and for T(Al^{3+}) modes in grossular between about 240 and 470 cm^{-1} (McAloon and Hofmeister 1993).

Other higher wavenumber OH^- bands can be observed in the spectra some water-poor andradites such as that shown in Fig. 9 given by the mode that 3605 cm^{-1} at 333 K. Moreover, an OH^--band with a wavenumber of 3612 (±1) cm^{-1} can be observed as part of a very broad OH^- absorption feature in the RT spectra of andradite crystals that contain a significant amount of the $Ca_3Fe^{3+}{}_2H_{12}O_{12}$ component (see Fig. 2 in Amthauer and Rossman 1998). We propose that the OH^- band at roughly 3612 cm^{-1} at RT in andradite-rich garnets (Table 2) could be related to the presence of finite-sized $Ca_3Fe^{3+}{}_2O_{12}H_{12}$-like clusters (Fig. 4a).

Finally, we propose, because andradite and grossular are so similar structurally that, in an analogous manner to the situation discussed above for hydrogrossular-like clusters in water-poor grossular, a series of different hydroandradite-like clusters may be present in some andradite crystals. They should be characterized by having OH^- stretching modes with energies between 3563 and 3606-3612 cm^{-1}. Consider, for example, the RT IR spectrum of "end-member" andradite 4282 (Fig. 11) that contains only 0.02 wt. % Al_2O_3 (Geiger et al. 2018 - see also similar spectrum

of andradite in Zhang et al. 2015). It is "untypical". Starting with the intense mode at 3561 cm^{-1} and moving to higher wavenumbers, one observes two OH^- modes at 3582 and 3595 cm^{-1}. We think they could represent the presence of two different hydroandradite-like clusters, whose exact $(H_4O_4)^{4-}$-group configuration (Fig. 4c-f) cannot be presently determined. Finally, in terms of this andradite garnet, the three modes at 3610, 3621 and 3633 cm^{-1} can be assigned to three hydrogrossular-like-clusters (Table 2).

We close this section by noting that many andradites and grossulars are not of "end-member" composition. There is often some degree of solid solution between the two and also to lesser degree with other common garnet components (e.g., $Fe^{2+}_3Al_2Si_3O_{12}$, $Mn^{2+}_3Al_2Si_3O_{12}$, $Mg_3Al_2Si_3O_{12}$). In order to address the issue of OH^- incorporation in calcium silicate garnets more fully, we need to consider the IR spectra of intermediate composition water-poor grossular-andradite crystals.

Intermediate composition and water-poor grossular-andradite garnets

Many, if not most, Ca-rich silicate garnets in Earth's crust are grossular-andradite solid solutions that crystallize during metamorphism. There can be complete $Al \Leftrightarrow Fe^{3+}$ exchange at [Y] across the join and the thermodynamic mixing behavior has been studied (Dachs and Geiger 2019). The cation mixing behavior can be complex because varying partial degrees in the long range order can occur, decreasing the space group symmetry below cubic (Takéuchi et al. 1982). At any rate, water-poor grossular-andradite garnets offer an additional system for investigation, because their temperatures of crystallization are well above those where many water-rich crystals are stable. What do their IR spectra show?

A number of IR spectra have been published (i.e., Rossman and Aines 1991; Phichaikamjornwut et al. 2012) and several garnets have been investigated in this work. Conceivably, it could be expected that spectral complexity could increase compared to the situation for end-member garnet species. The crystal chemistry of solid-solution garnets is more

complex because of Al^{3+}-Fe^{3+} mixing at [Y]. Local OH^- vibrational behavior could be affected, as discussed above (Fig. 2). Assuming statistically random Al^{3+}-Fe^{3+} mixing, there can be five possible local Y-cation configurations around a single, common $(H_4O_4)^{4-}$ group. They are: Al-Al-Al-Al, Fe^{3+}-Al-Al-Al, Fe^{3+}-Fe^{3+}-Al-Al, Fe^{3+}-Fe^{3+}-Fe^{3+}-Al, and Fe^{3+}-Fe^{3+}-Fe^{3+}-Fe^{3+}. For the case of strict random mixing, the probability for each of the five configurations is a function of the bulk composition of the crystal. The situation becomes more complex, if additional $(H_4O_4)^{4-}$ groups are brought into the analysis. Suffice it to note that a number of different energy OH^--stretching modes could potentially occur.

What is observed in the available IR spectra? To begin, many binary composition, water-poor, $Ca_3(Al_x,Fe^{3+}_{1-x})_2Si_3O_{12}$, garnets show an OH^- mode at 3563 cm^{-1} at RT. Following the analysis for the case of "end-member" andradite, it can be assigned to single, isolated $(H_4O_4)^{4-}$ group surrounded by Fe^{3+} cations. Clearly, the spectra of a number of the Fe^{3+}-bearing grossulars in Rossman and Aines (1991) show the presence of an OH^- band at about 3563 cm^{-1} (Their figures 4, 5, 6, 8, 9, 10 and samples 1125, 936, 1042, 1051, 1430, 938, 1327, 1357, and 1411, for example). The same is true for the IR spectra of several grossular-andradite garnets in Phichaikamjornwut et al. (2012). In addition, OH^- modes at 3581 and 3594 cm^{-1} are also observed in the spectra of some these grossular-andradite composition garnets with the assignments given above and in Table 2.

Take two specific examples, the first being garnet 6741 (Table 1) of approximate composition Gro73And23. Its IR spectrum was recorded at RT and 80 K (Fig. 12a). At RT three distinct and relatively strong OH^- bands are observable (i.e., 3688, 3666, and 3629 cm^{-1}) and at 80 K four bands (i.e., 3694, 3672, 3634, and 3615 cm^{-1}). Weak bands (i.e., 3565 cm^{-1} at RT and 3562 cm^{-1} at 80 K) and shoulders can also be discerned. In the case of this garnet, it is important to bear in mind that, although it has a considerable 25% andradite component, nearly all of the OH^- is contained in various hydrogrossular-like clusters. The simplest interpretation is that the energetics associated with the formation of hydrogrossular-like clusters are more favorable than for

hydroandradite-like clusters. This proposal is consistent with synthesis experiment results (Flint et al. 1941; Dilnesa et al. 2014) for garnets in the system $Ca_3Al_2(SiO_4)_3$-$Ca_3Al_2(H_4O_4)_3$-$Ca_3Fe^{3+}_2(SiO_4)_3$-$Ca_3Fe^{3+}_2(H_4O_4)_3$ as shown in Fig. 1. Only the binary $Ca_3Al_2(SiO_4)_3$-$Ca_3Al_2(H_4O_4)_3$ shows complete solid solution from end-member to end-member.

Finally, consider the RT spectrum of an andradite garnet of composition And76Gr23 (sample KPK 56-12-9 of Phichaikamjornwut et al. 2012) shown in Fig. 12b. It shows three strong OH^- bands with the two lowest wavenumber ones occurring at 3562 and 3582 cm^{-1}. They are associated with hydroandradite-like clusters (Table 2). The mode at 3611 cm^{-1} is difficult to assign and could represent an end-member katoite-like or a hydroandradite-like cluster (Table 2). The various weak bands, observable at higher wavenumbers, probably represent hydrogrossular clusters present in small amounts. At any rate, the bulk of the OH^- in this solid-solution garnet is partitioned into hydroandradite-like clusters. Research needs to be done to determine the nature of H_2O partitioning and hydrogarnet cluster formation in the nominally anhydrous system $Ca_3(Al_x,Fe^{3+}_{1-x})_2Si_3O_{12}$. In other words, the role of garnet composition with regards to the nature of structural "water" needs to be investigated as a function of P_{H_2O} and T.

IMPLICATIONS

Considerable and diverse research has been undertaken on various "water"-bearing garnets over the last approximate three decades. And, here, it should be noted that in terms of the many "end-member" grossular samples that have been studied by IR spectroscopy, that we are not aware of any "water"-free crystals. This is an important observation. Much has been learned, but much is still not understood. What is presently the state of the field and what needs to be done?

Previously, the IR and Raman spectra of different composition calcium silicate garnets could not be interpreted in any systematic and rational manner. Spectroscopic interpretation was often speculative with no rigorous scientific basis or it was simply not undertaken. It appears that proposals linking the large number of observed OH^- bands to different atomic mechanisms

involving "defects" or "non-standard" garnet elements (see Part II – Geiger and Rossman, this volume) are probably not fully correct. That is, chemistry and various defects were taken as the deciding factor in the nature of OH^- incorporation in many garnets. The model analysis presented here, if correct, simplifies the nature of OH^--substitution, by returning back to the central importance of the well-known hydrogarnet substitution, namely $(H_4O_4)^{4-} \Leftrightarrow (SiO_4)^{4-}$ or $(4H)^+ \Leftrightarrow (Si)^{4+}$. The varying and complex IR spectra of different calcium silicate garnets reflect the presence of various local microscopic- and nano-size $Ca_3Al_2H_{12}O_{12}$- and $Ca_3Fe^{3+}{}_2H_{12}O_{12}$-like clusters. Inclusion phases, probably hydrous layer silicates, can also give rise to OH^- bands. This is not to say, and we want to emphasize, that other OH^- substitutional mechanisms cannot occur in silicate garnet.

Open questions regarding spectroscopy remain. Intense OH^- bands at wavenumbers less than 3560 cm^{-1} are often observed in IR spectra of garnet. Further research is needed to interpret and assign them. It is needs to be determined if there are different IR absorption coefficients associated with the different modes. A crystal-chemical question that arises, is how OH^- can be incorporated in certain, other nominally anhydrous silicates? Could proton clustering play a role in any of them as well? A number of more mineralogical, petrological and geochemical issues remain to be studied. Concluding, it goes without saying that research on garnet has entered a new phase. Further issues relating to "water" in Ca silicate garnets are discussed in Part II (Geiger and Rossman this volume) of this investigation.

ACKNOWLEDGMENTS

Dr. B. Lothenbach kindly supplied the synthetic hydrogarnets and Dr. B. Phichaikamjornwut provided her IR data on grossular and andradite garnets for analysis. Dr. E. Grew assisted in constructing Fig. 1. This research was supported by grants from the Austrian Science Fund (FWF: P 30977-NBL) to C.A.G. and NSF (EAR-1322082) to G.R.R. C.A.G. also thanks the "Land

Salzburg" for financial support through the initiative "Wissenschafts- und Innovationsstrategie Salzburg 2025". Dr. E. Libowitzky made constructive comments that improved the manuscript.

596
597 **REFERENCES**

598 Adamo, I., Gatta, G.D., Rotiroti, N., Diella, V., and Pavese, A. (2011) Green andradite stones:
599 gemmological and mineralogical characterisation. European Journal of Mineralogy, 23, 91-
600 100.
601 Aines, R.D. and Rossman, G.R. (1984) The hydrous component in garnets: pyralspites. American
602 Mineralogist, 69, 1116-1126.
603 Albrecht, R., Hunger, J., Doert, T., and Ruck, M. (2019) Syntheses, crystal structures and physical
604 properties of chromium and rhodium hydrogarnets $Ca[Cr(OH)_6]_2$, $Sr[Cr(OH)_6]_2$, and
605 $Sr[Rh(OH)_6]_2$. European Journal of Inorganic Chemistry, 10, 1398-1405.
606 Amthauer, G. and Rossman, G.R. (1998) The hydrous component in andradite garnet. American
607 Mineralogist, 83, 835-840.
608 Armbruster, T. (1995) Structure refinement of hydrous andradite $Ca_3Fe_{1.54}Mn_{0.20}Al_{0.26}(SiO_4)_{1.65}$
609 $(O_4H_4)_{1.35}$, from the Wessels mine, Kalahari manganese field, South Africa. European
610 Journal of Mineralogy, 7, 1221-1225.
611 Armbruster, T. and Geiger, C.A. (1993) Andradite crystal chemistry, dynamic X-site disorder and
612 strain in silicate garnets. European Journal of Mineralogy, 5, 59-71.
613 Basso, R. and Cabella R. (1990) Crystal chemical study of garnets from metarodingites in the
614 Voltri Group metaophiolites (Ligurian Alps, Italy). Neues Jahrbuch für Mineralogie –
615 Monatshefte, 3, 127-136.
616 Basso, R. Cimmino, F., and Messiga, B. (1984) Crystal chemistry of hydrogarnets from three
617 different microstructural sites of a basaltic metarodingite from the Voltri Massif (Western
618 Liguria, Italy). Neues Jahrbuch für Mineralogie – Abhandlungen, 148, 246-258.
619 Bell, D.R. and Rossman, G.R. (1992) Water in Earth's mantle: The role of nominally anhydrous
620 minerals. Science, 255, 1391-1397.
621 Belyankin D.S. and Petrov, V.P. (1939) Hibschite in Georgia. Doklady of the Academy of
622 Sciences, U.S.S.R. 24, 349-352.

623 Belyankin, D.S. and Petrov, V.P. (1941a) Reexamining the chemical formula of hibschite.
624 Doklady of the Academy of Sciences, U.S.S.R. 30, 66-68.
625 Belyankin, D.S. and Petrov, V.P. (1941b) The grossularoid group (hibschite, plazolite). American
626 Mineralogist, 26, 450-453.
627 Beran, A., Sturma, R. and Zemann, J. (1983) Ultrarotspektroskopische Untersuchungen über den
628 OH-Gehalt einiger Granate. Österreichische Akademie der Wissenschaften, Mathmatisch-
629 naturwissenschafte Klasse, 75-79.
630 Birkett, T.C. and Trzcienski, Jr., W.E. (1984) Hydrogarnet: Multi-site hydrogen occupancy in the
631 garnet structure. Canadian Mineralogist, 22, 675-680.
632 Carlson, E.T. (1956) Hydrogarnet formation in the system lime-alumina-silica-water. Journal of
633 Research of the National Bureau of Standards, 56, 327-335.
634 Cho, H. and Rossman, G.R. (1993) Single-crystal NMR studies of low-concentration hydrous
635 species in minerals: Grossular garnet. American Mineralogist, 78, 1149-1164.
636 Cohen-Addad, C., Ducros, P., and Bertaut, E.F. (1967) Étude de la substitution du groupement
637 SiO_4 par $(OH)_4$ dans les composés $Al_2Ca_3(OH)_{12}$ et $Al_2Ca_3(SiO_4)_{2.16}(OH)_{3.36}$ de type
638 grenat. Acta Crystallographica, 23, 220-230.
639 Cornu, F. (1905) “Hibschit” aus Einschlüssen des oberturonen Kalkmergels der Cuvieristufe im
640 Phonolit des Marienberges bei Aussig. Tschermaks mineralogische und petrographische
641 Mitteilungen, 24, 327-328.
642 Cornu, F. (1906) Hibschit, ein neues Kontaktmineral. Tschermaks mineralogische und
643 petrographische Mitteilungen, 25, 249-268.
644 Dachs, E. and Geiger, C.A. (2019) Thermodynamic behaviour of grossular–andradite,
645 $Ca_3(Al_xFe^{3+}_{1-x})_2Si_3O_{12}$, garnets: a calorimetric study. European Journal of Mineralogy, 31,
646 443-451.
647 Dachs, E., Geiger, C.A., Benisek, A., and Grevel, K-D. (2012) Grossular: A crystal-chemical,
648 calorimetric, and thermodynamic study. American Mineralogist, 97, 1299-1313.

649 Dilnesa, B.Z., Lothenbach, B., Renaudin, G., Wichser, A., and Kulik, D. (2014) Synthesis and
650 characrterization of $Ca_3(Al_xFe_{1-x})_2(SiO_4)_y(OH)_{4(3-y)}$. Cement and Concrete Research, 59,
651 96-111.
652 Ferro, O., Galli, E., Papp, G., Quartieri, S., Szakáll, S., and Vezzalini, G. (2003) A new occurrence
653 of katoite and re-examination of the hydrogrossular group. European Journal of
654 Mineralogy, 15, 419-426.
655 Flint, E.P. and Wells, L.S. (1941) Relationship of the garnet-hydrogarnet series to the sulfate
656 resistance of portland cement. Journal of Research of the National Bureau of Standards, 27,
657 Research Paper RP 1411, 171-180.
658 Flint, E.P., McMurdie, H.F., and Wells, L.S. (1941) Hydrothermal and X-ray studies of the garnet-
659 hydrogarnet series and the relationship of the series to hydration products of portland
660 cement. National Bureau of Standards, Research, 26, Paper RP 1335, 13-33.
661 Foreman, D.W., Jr. (1968) Neutron and X-ray diffraction study of $Ca_3Al_2(O_4D_4)_3$, a garnetoid. The
662 Journal of Chemical Physics, 48, 3037-3041.
663 Foshag, W.F. (1920) Plazolite, a new mineral. American Mineralogist. 5, 183-185.
664 Geiger, C.A. (1998) A powder infrared spectroscopic investigation of garnet binaries in the system
665 $Mg_3Al_2Si_3O_{12}$-$Fe_3Al_2Si_3O_{12}$-$Mn_3Al_2Si_3O_{12}$-$Ca_3Al_2Si_3O_{12}$. European Journal of Mineralogy,
666 3, 407-422.
667 Geiger, C.A. (2008) Silicate garnet: A micro to macroscopic (re)view. American Mineralogist. 93,
668 360-372.
669 Geiger, C.A. (2013) Garnet: A key phase in nature, the laboratory and in technology. Elements, 9,
670 447-452.
671 Geiger, C.A. and Armbruster, T. (1997) $Mn_3Al_2Si_3O_{12}$ spessartine and $Ca_3Al_2Si_3O_{12}$ grossular
672 garnet: dynamical structural and thermodynamic properties. American Mineralogist, 82,
673 740-747.
674 Geiger, C.A. and Rossman, G.R. (2018) IR spectroscopy and OH^- in silicate garnet: The long
675 quest to document the hydrogarnet substitution. American Mineralogist, 103, 384-393.

676 Geiger, C.A. and Rossman, G.R. (this volume) Micro- and nano-size hydrogarnet clusters in
677 calcium silicate garnet: Part II. mineralogical, petrological and geochemical aspects.
678 American Mineralogist.
679 Geiger, C.A. and Rossman, G.R. (submitted – 2019c) Pyrope from the Dora Maira Massif,
680 Western Alps: Water in the hydrogrossular. Contributions to Mineralogy and Petrology.
681 Geiger, C.A. and Rossman, G.R. (in prep. – 2019d) Hydrogarnet clusters and proton ordering in
682 spessartine: The continuing quest to understand H_2O in garnet.
683 Geiger, C.A., Dachs, E., Vielreicher, N., and Rossman, G.R. (2018) Heat capacity and entropy
684 behavior of andradite: A multi-sample and -methodological investigation. European
685 Journal of Mineralogy, 30, 681-694.
686 Grew, E.S., Locock, A.J., Mills, S.J., Galuskina, I.O., Galuskin, and E.V., Hålenius, U. (2013)
687 Nomenclature of the garnet supergroup. American Mineralogist, 98, 785-811.
688 Harmon, K.M., Gabriele, J.M., and Nuttall, A.S. (1982) Hydrogen bonding in the tetrahedral
689 $O_4H_4^{4-}$-cluster in hydrogrossular. Journal of Molecular Structure, 82, 213-219.
690 Heller-Kallai, L., Yariv, S., and Gross, S. (1975) Hydroxyl-stretching frequencies of serpentine
691 minerals. Mineralogical Magazine, 40, 197-200.
692 Hofmeister, A.M. and Chopelas, A. (1991) Vibrational spectroscopy of end-member silicate
693 garnets. Physics and Chemistry of Minerals, 17, 503-526.
694 Hsu, L.C. (1980) Hydration and phase relations of grossular-spessartine garnets at P_{H_2O} = 2 Kb.
695 Contributions to Mineralogy and Petrology, 71, 407-415.
696 Ingrin, J. and Skogby, H. (2000) Hydrogen in nominally anhydrous upper-mantle minerals:
697 concentration levels and implications. European Journal of Mineralogy, 12, 543-570.
698 Ito, J. and Frondel, C. (1967) New synthetic hydrogarnets. American Mineralogist, 52, 1105-1109
699 Jappy, T.G. and Glasser, F.P. (1991/92) Synthesis and stability of silica-substituted hydrogarnet
700 $Ca_3Al_2Si_{3-x}O_{12-4x}(OH)_{4x}$. Advances in Cement Research, 4, 1-8.
701 Kobayashi, S. and Shoji, T. (1983) Infrared analysis of the grossular-hydrogrossular series.
702 Mineralogical Journal, 11, 331-343.

703 Kolesov, B.A. and Geiger, C.A. (1998) Raman spectra of silicate garnets. Physics and Chemistry
704 of Minerals, 25, 142-151.
705 Kolesov, B.A. and Geiger, C.A. (2005) The vibrational spectrum of synthetic hydrogrossular
706 (Katoite) $Ca_3Al_2(O_4H_4)_3$: A low temperature IR and Raman spectroscopic study. American
707 Mineralogist, 90, 1335-1341.
708 Kresten, P., Nairis, H.J., and Wadsten, T. (1982) Hydroandradite from Alnö Island, Sweden.
709 Geologiska Föreningens i Stockholm Förhandlingar, 104, 240.
710 Kurka, A., Blanchard, M., and Ingrin, J. (2005) Kinetics of hydrogen extraction and deuteration in
711 grossular. Mineralogical Magazine, 69, 359-371.
712 Kuzel, H.-J. (1968) Über die Diadochie von Al^{3+}, Cr^{3+}, und Fe^{3+} in $3CaO \cdot Al_2O_3 \cdot 6H_2O$ oberhalb
713 50° C. Neues Jahrbuch für Mineralogie, Monatshefte. 87-96.
714 Lager, G.A. and von Dreele, R.B. (1996) Neutron powder diffraction study of hydrogarnet to 9.0
715 GPa. American Mineralogist, 81, 1097-1104.
716 Lager, G.A., Armbruster, T., and Faber, G. (1987) Neutron and X-ray diffraction study of
717 hydrogarnet $Ca_3Al_2(O_4H_4)_3$. American Mineralogist, 72, 756-765.
718 Lager, G.A., Downs, R.T., Origlieri, M., and Garoutte, R. (2002) High-pressure single-crystal X-
719 ray study of katoite hydrogarnet: Evidence for a phase transition from $Ia3d \rightarrow I43d$
720 symmetry at 5 GPa. American Mineralogist, 87, 642-647.
721 Maldener, J., Hösch, A., Langer, K., and Rauch, F. (2003) Hydrogen in some natural garnets
722 studied by nuclear reaction analysis and vibrational spectroscopy. Physics and Chemistry
723 of Minerals, 30, 337-344.
724 McAloon, B.P. and Hofmeister, A.M. (1993) Single-crystal absorption and reflection infrared
725 spectroscopy of birefringent grossular-andradite garnets. American Mineralogist, 78, 957-
726 967.
727 Mellini, M., Fuchs, Y., Viti, C., Lemaire, C., and Linarès, J. (2002) Insights into the antigorite
728 structure from Mössbauer and FTIR spectroscopies. European Journal of Mineralogy, 14,
729 97-104.

730 Moore, R.K., White, W.B., and Long, T. (1971) Vibrational spectra of the common silicates: I.
731 The garnets. American Mineralogist, 56, 54-71.
732 Nakamoto, K. (2009) Infrared and Raman Spectra of Inorganic and Coordination Compounds,
733 Part A: Theory and Applications in Inorganic Chemistry. John Wiley and Sons, Inc. 6th
734 edition, 419 p.
735 Novak, G.A. and Gibbs, G.V. (1971) The crystal chemistry of the silicate garnets. American
736 Mineralogist, 56, 791-825.
737 Orlando, R., Torres, F.J., Pascale, F., Ugliengo, P., Zicocvich-Wilson, C., and Dovesi, R. (2006)
738 Vibrational spectrum of katoite $Ca_3Al_2[(OH)_4]_3$: A periodic ab initio study. Journal of
739 Physical Chemistry B, 110, 692-701.
740 Pabst, A. (1942) Reexamination of hibschite. American Mineralogist, 27, 783-792.
741 Passaglia, E. and Rinaldi, R. (1984) Katoite, a new member of the $Ca_3Al_2(SiO_4)_3$-$Ca_3Al_2(OH)_{12}$
742 series and a new nomenclature for the hydrogrossular group of minerals. Bulletin de
743 Minéralogie, 107, 605-618.
744 Peslier, A.H. (2010) A review of water contents of nominally anhydrous natural minerals in the
745 mantles of Earth, Mars and the Moon. Journal of Volcanology and Geothermal Research,
746 197, 239-258.
747 Phichaikamjornwut, B., Skogby, H., Ounchanum, P., Limtrakun, P., and Boonsoong, A. (2012)
748 Hydrous components of grossular-andradite garnets from Thailand: thermal stability and
749 exchange kinetics. European Journal of Mineralogy, 24, 107-121.
750 Pistorius, C.W.F.T and Kennedy, G.C. (1960) Stability relations of grossularite and
751 hydrogrossularite at high temperatures and pressures. American Journal of Science, 258,
752 247-257.
753 Reynes, J., Jollands, M., Hermann, J., and Ireland (2018) Experimental constraints on hydrogen
754 diffusion in garnet. Contributions to Mineralogy and Petrology, 173, 23.
755 Rossman, G.R. and Aines, R.D. (1986) Spectroscopy of a birefringent grossular from Asbestos,
756 Quebec, Canada. American Mineralogist, 71, 779-780.

Rossman, G.R. and Aines, R.D. (1991) The hydrous components in garnets: Grossular-hydrogrossular. American Mineralogist, 76, 1153-1164.

Schroeder, P.A. (2002) Infrared Spectroscopy in clay science. In CMS Workshop Lectures, Vol. 11, Teaching Clay Science, A. Rule and S. Guggenheim, eds., The Clay Mineral Society, 181-206.

Takéuchi, Y., Haga, N., Umizu, S., and Sato, G. (1982) The derivative structure of silicate garnets in grandite. Zeitschrift für Kristallographie, 158, 53-99.

Thorvaldson, T. and Grace, N.S. (1929) The hydration of the aluminates of calcium. I. A new crystalline form of hydrated tricalcium aluminate. Canadian Journal of Research, 1, 36-47.

Thorvaldson, T., Grace, N.S., and Vigfusson, V.A. (1929) The hydration of the aluminates of calcium. II. The hydration products of tricalcium aluminate. Canadian Journal of Research, 1, 201-213.

Wilkins, R.W.T. and Sabine, W. (1973) Water content of some nominally anhydrous silicates. American Mineralogist, 58, 508-516.

Withers, A.C., Wood, B.J., and Carroll, M.R. (1998) The OH content of pyrope at high pressure. Chemical Geology, 147, 161-171.

Woodford, A.O., Crippen, R.A., and Garner, K.B. (1941) Section across Commercial quarry, Crestmore, California. American Mineralogist, 26, 351-381.

Wright, K., Freer, R., and Catlow, C.R.A. (1994) The energetics and structure of the hydrogarnet defect in grossular: A computer simulation study. Physics and Chemistry of Minerals, 20, 500-503.

Yoder, H.S., Jr. (1950) Stability relations of grossularite. The Journal of Geology, 58, 221-253.

Zhang, P., Ingrin, J., Depecker, C., and Xia, Q. (2015) Kinetics of deuteration in andradite and garnet. American Mineralogist, 100, 1400-1410.

This is a preprint, the final version is subject to change, of the American Mineralogist (MSA)
Cite as Authors (Year) Title. American Mineralogist, in press.
DOI: https://doi.org/10.2138/am-2020-7256

781 Table 1. Description of natural and synthetic grossular, andradite, grossular-andradite, and hydrogarnet samples measured or used in this study.

Garnet Type & Sample Label	Type/Locality (Source)	Sample Description (*P-T*, color, thickness, source)	Approximate Garnet Composition
Grossular	Synthetic grossular (C.A. Geiger)	T = 800 °C and P_{H_2O} = 0.2 GPa; 0.38 mm; Geiger & Armbruster (1997)	Gross100
Gr83	Synthetic grossular	T = 1000 °C and P_{H_2O} = 3.0 GPa; Digitalized data from Fig. 1 in Withers et al. (1998) normalized to 1 mm thickness	Gross100
Grossular GRR 53	Asbestos, Quebec, Canada (Shale's Lapidary)	Pale orange, "Hessonite", 0.139 mm; Rossman & Aines (1991)	Gross94Andr06
Grossular GRR 1038	Jeffrey Mine, Asbestos, Quebec, Canada (Rock H. Currier, Jewel Tunnel Imports)	Colorless rim, green colored core (Cr^{3+}), 0.276 mm; Rossman & Aines (1991)	Gross96Andr04
Grossular GRR 1042	Vesper Peak, Snohomish Co., WA, USA (Caltech collection, CIT-8197)	Orange-brown, 1.156 mm; Rossman & Aines (1991)	Gross86Andr14

Grossular GRR 1058	Synthetic hydrogrossular (G. Lager)	Synthetic (#GL IV 2Sia), KBr pellet; Lager et al. (1987); Rossman & Aines (1991)	$Ca_3Al_2(O_4H_4)_3$
Grossular GRR 1059	Synthetic hydrogrossular (G. Lager)	Synthetic (#Gl VII 1), KBr pellet; Lager et al. (1987); Rossman & Aines (1991)	$Ca_3Al_2(SiO_4)_{2.28}(O_4H_4)_{0.72}$
Grossular GRR 1285	Jeffrey Mine, Asbestos, Quebec, Canada (F. Allen)	0.030 mm; light orangish pink; Cho & Rossman (1993); Allen and Buseck (1998)	Gross98Andr02
Grossular GRR 1329	Commercial Quarry, Crestmore, CA, USA (Pomona College, R.A. Crippen, #RAC U-29)	Near-colorless "plazolite". Braided veins between gehlenite, ~12 um thick; Woodford et al. (1941), Rossman & Aines (1991)	-
Grossular GRR 1358	Commercial Quarry Crestmore, CA, USA (R. Basso - orginally from A. Pabst)	Colorless "Plazolite", 0.024 mm thick; Pabst (1942); Rossman & Aines (1991)	$Ca_3Al_2(SiO_4)_{1.82}(O_4H_4)_{1.18}$
Grossular 1386	Merelani Hills, Lelatema Mountains, Umba Valley, Aursha Region, Tanzania (Peter Flusser, Overland Gems, Los Angeles)	Nearly colorless, ~5 mm gemmy, water-worn, crystal fragment; Cho & Rossman (1993); Palke et al. (2015)	Gross99Andr01
Grossular 1420	Rauris Valley, Salzburger-Land, Austria	Orange crystals, 0.186 mm thick;	Gross75Andr25

	(Caltech collection CIT-12534)	Rossman & Aines (1991)	
Grossular 1424	Garnet Queen Mine (?), Santa Rosa Mountains, San Diego County, CA, USA (Caltech collection, CIT-8804)	Orange crystals, 0.518 mm thick; Rossman & Aines (1991)	Gross88Andr12
Grossular GRR 1430.2	Belvidere Mountain, Eden Mills, Vermont (F. Allen)	Moderate orange crystals, 1.381 mm thick; Rossman & Aines (1991)	Gross94Andr06
Grossular GRR 1444	Pietra Massif, Montalto di Castro, Viterbo, Lazio, Italy (E. Passaglia)	Katoite, micro KBr pellet; Passaglia & Rinaldi (1984)*; Rossman & Aines (1991)	$Ca_{2.96}(Al_{1.85}Mg_{0.01})(Si_{0.69}S_{0.11})O_{2.93}(OH)_{9.07}$*
Andradite GRR 1263	San Benito Co., CA, USA (collected by GRR)	Black, serpentinite, 0.260 mm; Amthauer & Rossman (1998)	Andr99
Andradite 4282	Madagascar? (Ebay – Zoultier.com)	Light green transparent crystal, anisotropic, 0.606 mm; Geiger et al. (2018)	Andr99
Grossular-Andradite 6741	Africa (Ebay)	Greenish yellow, Anisotropic sector zoning and bands observed under crossed, 0.617 mm;	Gross73Andr23

		Dachs & Geiger (2019)	
Andradite-Grossular KPK 56-12-9	Phu Kha Hill, Mueang District, Lop Buri Province, Thailand (IR results B. Phichaikamjornwut)	Yellowish green to brownish green, 0.5-3 mm diameter crystals, skarn; Phichaikamjornwutet et al. (2012)	Andr73Gross26
Synthetic Hydrogarnet	(B. Lothenbach)	Very fine-grain; Dilnesa et al. (2014)	$Ca_3Al_2(SiO_4)(O_4H_4)_2$
Synthetic Hydrogarnet	(B. Lothenbach)	Very fine-grain; Dilnesa et al. (2014)	$Ca_3(Al_{1.4},Fe^{3+}_{0.6})_2(SiO_4)(O_4H_4)_2$
Synthetic Hydrogarnet	(B. Lothenbach)	Very fine-grain; Dilnesa et al. (2014)	$Ca_3(Al_{1.0},Fe^{3+}_{1.0})_2(SiO_4)(O_4H_4)_2$
Synthetic Hydrogarnet	(B. Lothenbach)	Very fine-grain; Dilnesa et al. (2014)	$Ca_3(Al_{0.6},Fe^{3+}_{1.4})_2(SiO_4)(O_4H_4)_2$
Synthetic Hydrogarnet	(B. Lothenbach)	Very fine-grain; Dilnesa et al. (2014)	$Ca_3Fe^{3+}_2(SiO_4)_{0.75}(O_4H_4)_{2.25}$

This is a preprint, the final version is subject to change, of the American Mineralogist (MSA)
Cite as Authors (Year) Title. American Mineralogist, in press.
DOI: https://doi.org/10.2138/am-2020-7256

782 Table 2. OH^- stretching modes (greater than 3560 cm^{-1}) observed for calcium silicate garnets at room temperature, their assignment and cluster type.

Natural Grossulars* (cm^{-1})	Natural Andradite§ (cm^{-1})	Synthetic Grossular-Andradite-$Ca_3Al_2H_{12}O_{12}$-$Ca_3(Al,Fe^{3+})_2H_{12}O_{12}$ Garnets (cm^{-1})	Synthetic Grossular# (cm^{-1})	Synthetic Hydro/Andradite+ (cm^{-1})	Assignment	Crystal Chemistry Cluster Type
3684-3688	-	-	(3688)?	-	Hydrous inclusion phase	-
3674-3678	~3678	-	-	-	Hydrous inclusion phase	-
~3660	-	~3658	3666	-	Finite size katoite cluster	Fig. 4a
~3657	-	-	3660	-	Six $(H_4O_4)^{4-}$ Hydrogrossular cluster (?)	Fig. 4g
~3641	-	-	3645	-	Five $(H_4O_4)^{4-}$ Hydrogrossular cluster	Fig. 4f
~3634	~(3632)	-	3633	-	Four $(H_4O_4)^{4-}$ Hydrogrossular cluster	Fig. 4e
~3622	~(3621)	-	3623	-	Three $(H_4O_4)^{4-}$ Hydrogrossular cluster	Fig. 4d
~3612	~(3611)?	-	3613	-	Two $(H_4O_4)^{4-}$ Hydrogrossular cluster	Fig. 4c
~3599	-	-	3604	-	One $(H_4O_4)^{4-}$ Hydrogrossular cluster	Fig. 4b
-	~3611?	~3611	-	3612	Finite size $Ca_3Fe^{3+}{}_2O_{12}H_{12}$ cluster (?)	Fig. 4a
~(3594)	~3594	-	-	-	Unspecified Hydroandradite cluster	?
~(3581)	~3581	-	(3579)?	-	Unspecified Hydroandradite cluster	?

This is a preprint, the final version is subject to change, of the American Mineralogist (MSA)
Cite as Authors (Year) Title. American Mineralogist, in press.
DOI: https://doi.org/10.2138/am-2020-7256

~(3563)	~3563	-	(3560)?	3563	One $(H_4O_4)^{4-}$ Hydroandradite cluster	Fig. 4b

*Varies from garnet to garnet and can be absent, [§]Geiger and Rossman (2018) and sample 4282, [#]this work from curve fit, [+]Geiger and Rossman (2018) and Amthauer and Rossman (1998) for synthetic $Ca_3Fe^{3+}_2(4H_{0.19}Si_{2.81})O_{12}$.

FIGURE CAPTIONS

Figure 1. The four-component system $Ca_3Al_2H_{12}O_{12}$-$Ca_3Fe^{3+}{}_2H_{12}O_{12}$-$Ca_3Fe^{3+}{}_2Si_3O_{12}$-$Ca_3Al_2Si_3O_{12}$ and the respective garnet nomenclature. The thick solid black lines indicate the degree of possible solid solution and the black dotted lines indicate uncertainty. There can be complete solid solution along the andradite-grossular and grossular-katoite binaries, but the full degree of solid solution along the $Ca_3Fe^{3+}{}_2H_{12}O_{12}$-andradite and katoite-$Ca_3Fe^{3+}{}_2H_{12}O_{12}$ joins is not known. The two gray dashed lines mark the 50:50 compositions of the four binary systems. The solid-solution behavior of the $Ca_3Fe^{3+}{}_2Si_3O_{12}$-$Ca_3Al_2H_{12}O_{12}$ and $Ca_3Al_2Si_3O_{12}$-$Ca_3Fe^{3+}{}_2H_{12}O_{12}$ binaries (gray dotted lines), as well as higher-order ternary or quaternary compositions, is also not understood.

Figure 2. Local atomic environment involving a single OH^- dipole in the case of calcium hydrogarnet (no Si cation). The oxygen anion is bonded to one Y(Al or Fe^{3+}) cation (blue), two X(Ca) cations (yellow - with bond lengths of Ca1-O(1) = 2.462(3) Å and Ca(2)-O(4) = 2.520(3) Å in hydrogrossular - Lager et al. 2002) and a H atom (pink).

Figure 3. IR single-crystal spectra in the energy range of the OH^- stretching vibrations for five natural and synthetic garnets along the join $Ca_3Al_2(H_4O_4)_3$-$Ca_3Al_2(SiO_4)_3$ as replotted from Rossman and Aines (1991). The sample labels (Table 1) and the number of Si atoms per formula unit (pfu) are given.

Figure 4. Various possible hydrogarnet-like clusters in grossular or andradite. H atoms are pink, SiO_4 groups are red and YO_6 groups with Y = Al^{3+} or Fe^{3+} are blue. Hydrogarnet (H_4O_4) "tetrahedra" are shown in green. The oxygen atoms located at the corners of the polyhedra and the X-cation are not shown for the sake of clarity. a.) Crystal-chemical environment for

811 end-member katoite hydrogarnet or a finite-sized katoite-like cluster, as given by the OH^-
812 stretching mode at about 3662 cm^{-1}. b.) Cluster arrangement involving a single $(H_4O_4)^{4-}$ group
813 and the rest by SiO_4 groups, as given by the OH^- stretching mode at about 3600 cm^{-1}. c.)
814 Cluster arrangement involving two $(H_4O_4)^{4-}$ groups and the rest SiO_4 groups, as given by the
815 mode at about 3611 cm^{-1}. d.) Cluster arrangement involving three $(H_4O_4)^{4-}$ groups and the rest
816 SiO_4 groups, as given by the mode at about 3622 cm^{-1}. e.) Cluster arrangement involving four
817 $(H_4O_4)^{4-}$ groups and the rest SiO_4 groups, as given by the mode at about 3633 cm^{-1}. f.) Cluster
818 arrangement involving five $(H_4O_4)^{4-}$ groups and a single SiO_4 group, as given by the mode at
819 about 3644 cm^{-1} and g.) Hypothetical cluster arrangement involving six $(H_4O_4)^{4-}$ groups, as
820 possibly given by the mode at about 3657 cm^{-1}.
821
822 Figure 5. a.) IR single-crystal spectra in the wavenumber range of the OH^- stretching
823 vibrations of synthetic "end-member" grossular normalized to 1 mm thickness (Geiger and
824 Armbruster 1997) and natural nearly end-member grossular GRR 53 (Table 1). b.) Fitted
825 spectrum of synthetic grossular.
826
827 Figure 6. IR single-crystal spectra in the energy range of the OH^- stretching vibrations at RT
828 of natural grossular GRR 1285 (intensity 3x) and synthetic grossular Gr83 (normalized to 1
829 mm thickness) of Withers et al. (1998). Samples described in Table1.
830
831 Figure 7. Stacked plot of different spectra of natural grossulars (Table 1) and the synthetic
832 hydrogarnet GRR 1059 showing OH^- modes at about 3560, 3583, 3599, 3612, 3622, 3633,
833 3643, 3657 and 3662 cm^{-1}. They are related to different microscopic- to nano-size
834 hydrogarnet clusters (see text). The mode at 3688 cm^{-1} may be due to tiny "serpentine
835 mineral" inclusions (see text).
836

Fig. 8. Supplementary figure. IR spectrum of grossular GRR 1386 (Table 1) and its curve fit. Note the OH^- modes at 3688 and 3674 cm^{-1}. They are possibly related to the presence of tiny inclusion phases of hydrous layer silicates and probably a "serpentine mineral" (see text).

Figure 9. Stacked plot of IR ATR powder spectra of five synthetic hydrogarnets as synthesized and described by Dilnesa et al. (2014).

Figure 10. IR single-crystal spectra in the energy range of the OH^- stretching vibrations at 333 K and 80 K of a natural "end-member" andradite GRR 1263 (Table 1).

Figure 11. IR single-crystal spectrum in the energy range of the OH^- stretching vibrations at RT of natural "end-member" andradite 4282 (Table 1) with fitted bands.

Figure 12. IR single-crystal spectra in the energy range of the OH^- stretching vibrations for: a.) sample 6741 of composition grossular73-andradite23 at 273 K and 80 K and b.) sample KPK 56-12-9 of composition andradite73-grossular26 at RT. Sample description in Table 1.

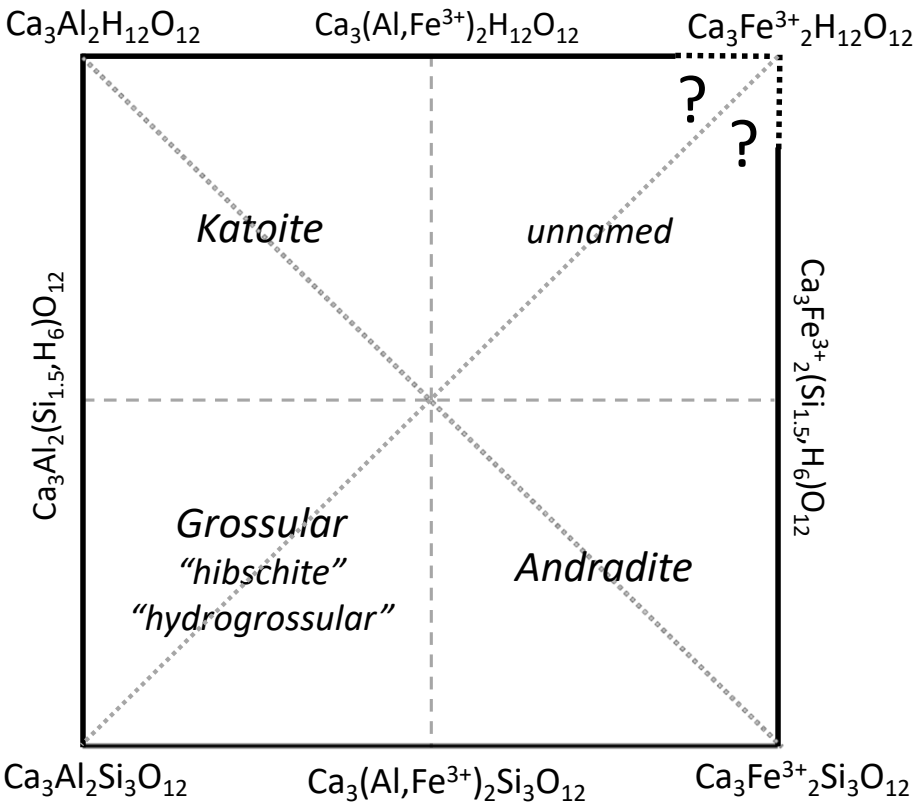

Figure 1.

866

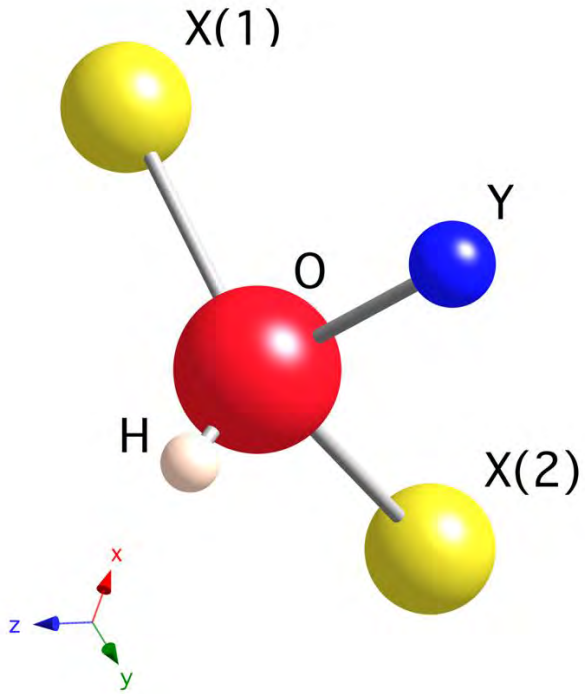

867

868

869

870

871

872

873

874 Figure 2.

875

876

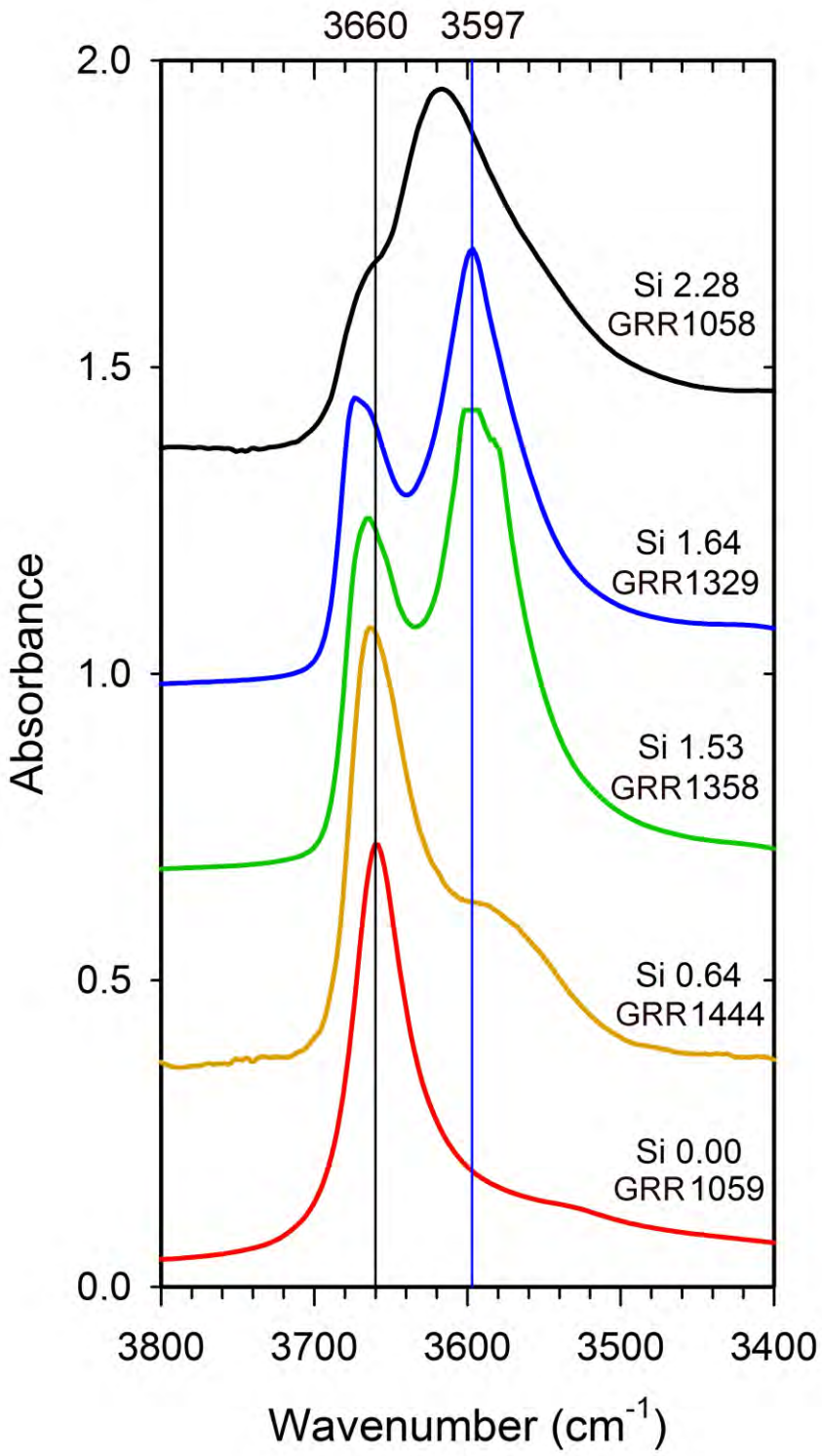

877

878

879

880 Figure 3.

881

882 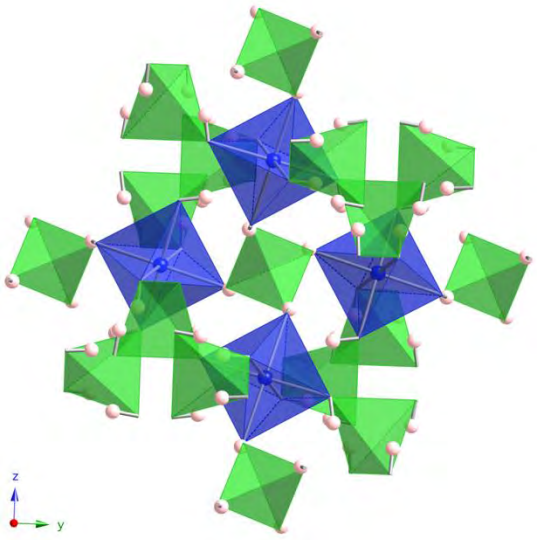 a. 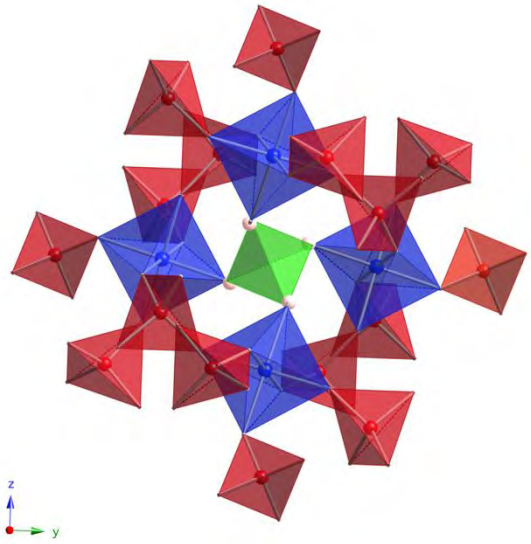 b.

883 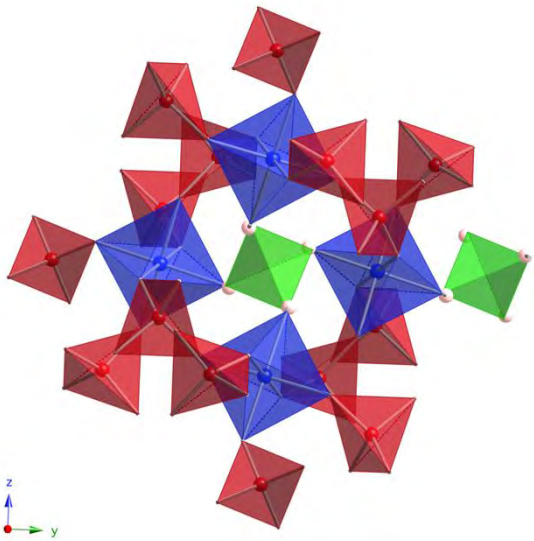 c. 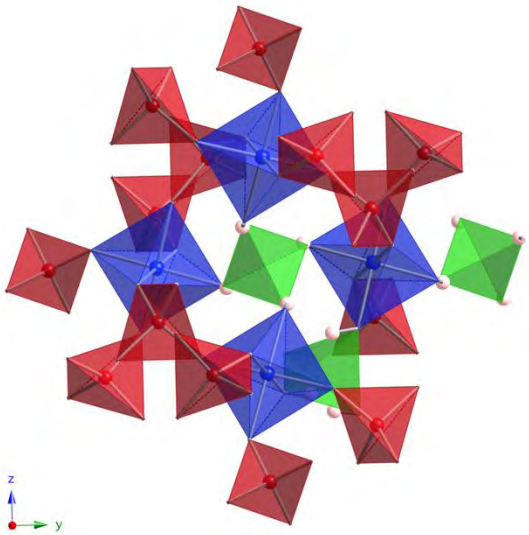 d.

884 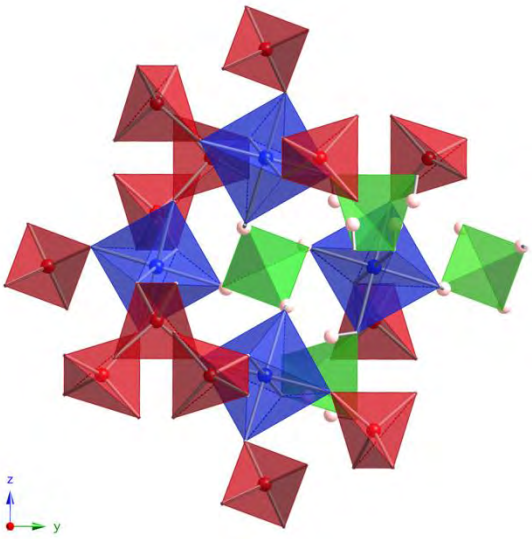 e. 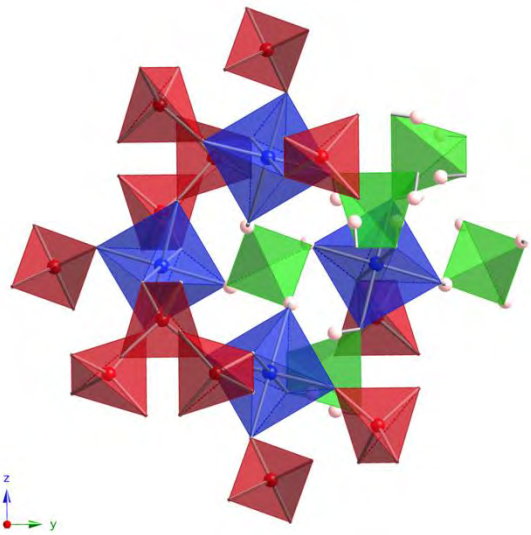 f.

885

886

887 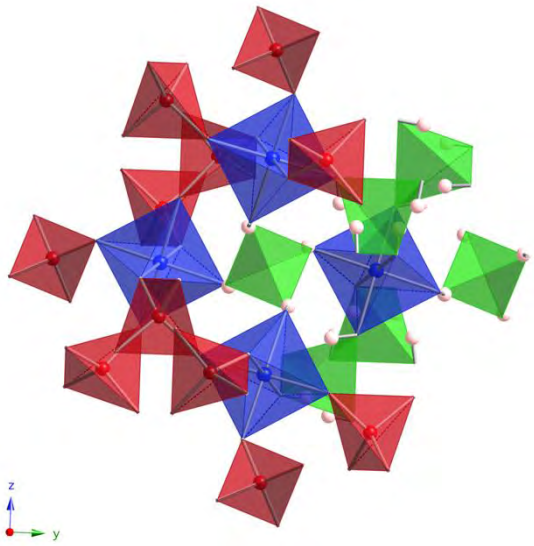

g.

888

889

890

891

892

893 Figure 4a, b, c, d, e, f and g.

894

895

896

897

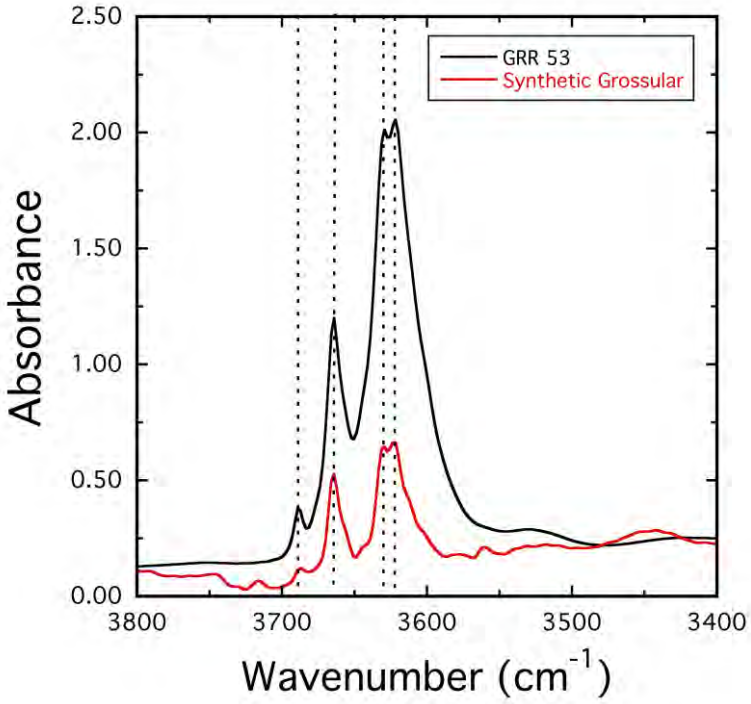

a.)

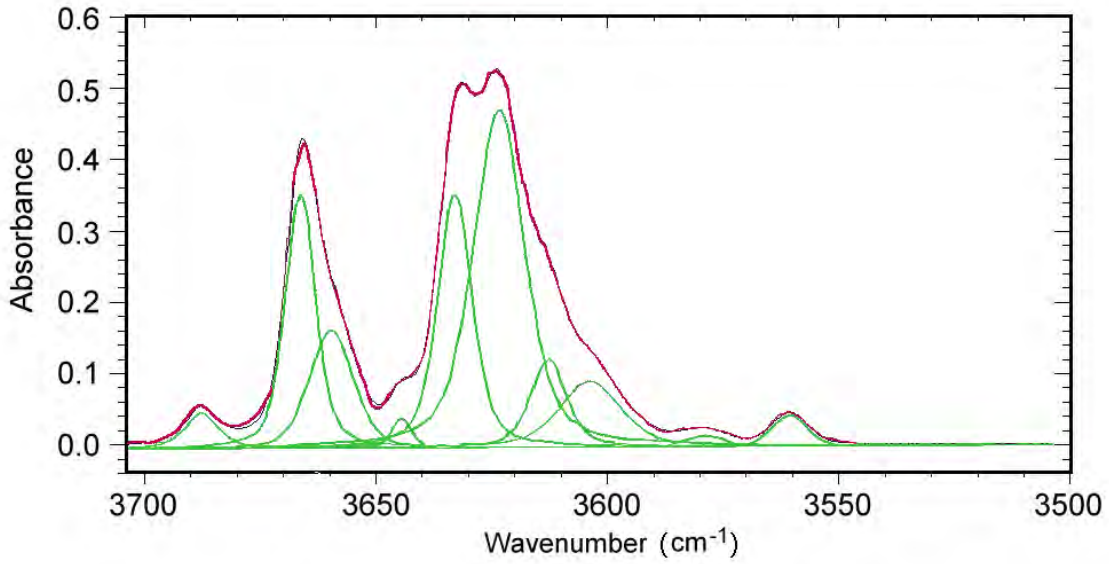

Curve Name	Centre	Width	Height	% Gaussian	Type	Area
Curve 1	3688	8.2	0.05	26	Mixed	0.59
Curve 2	3666	7.7	0.36	58	Mixed	3.51
Curve 3	3660	11.2	0.17	72	Mixed	2.26
Curve 4	3645	5.4	0.04	100	Mixed	0.24
Curve 5	3633	8.9	0.36	56	Mixed	4.08
Curve 6	3623	13.1	0.48	52	Mixed	8.14
Curve 7	3613	9.1	0.12	51	Mixed	1.46
Curve 8	3604	15.4	0.09	54	Mixed	1.85
Curve 9	3579	9.8	0.02	100	Mixed	0.16
Curve 10	3561	8.8	0.04	82	Mixed	0.44

b.)

Figure 5.

902

903

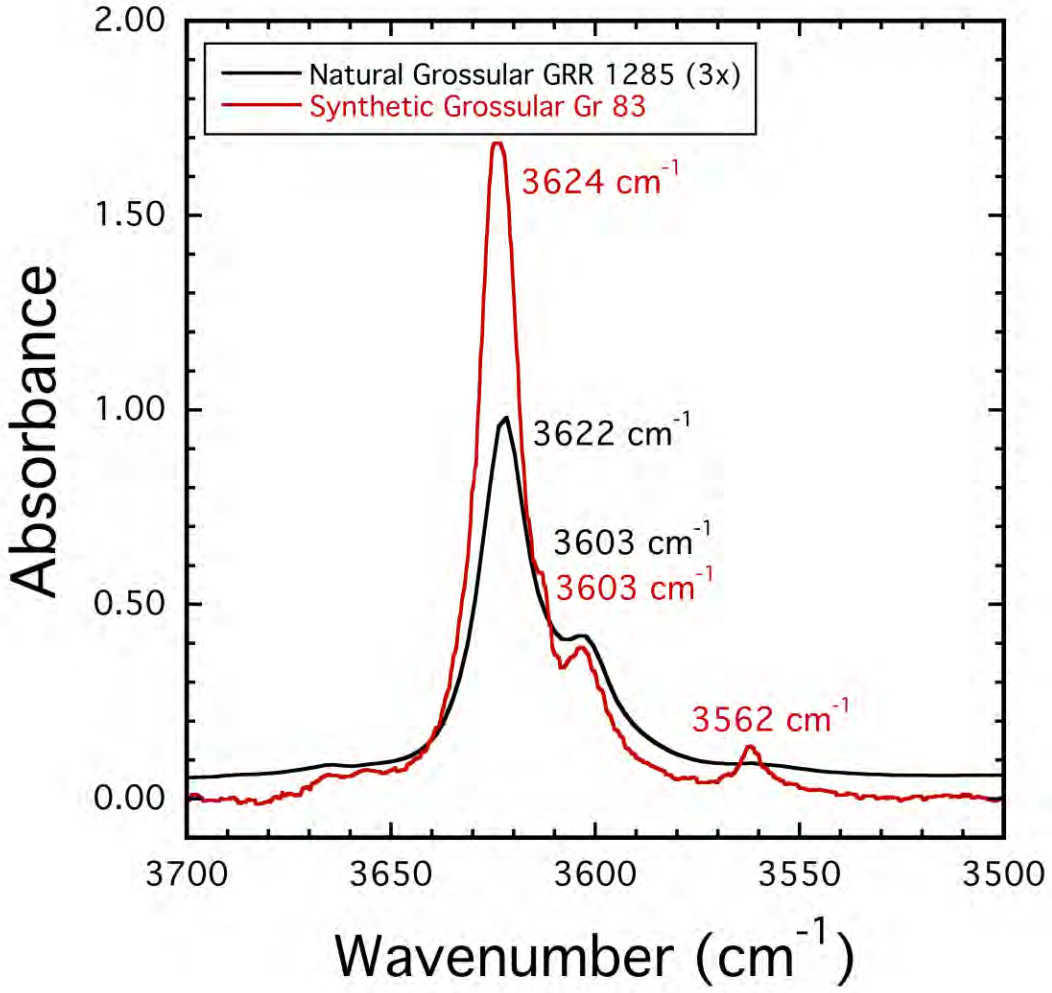

904

905

906

907

908 Figure 6.

909

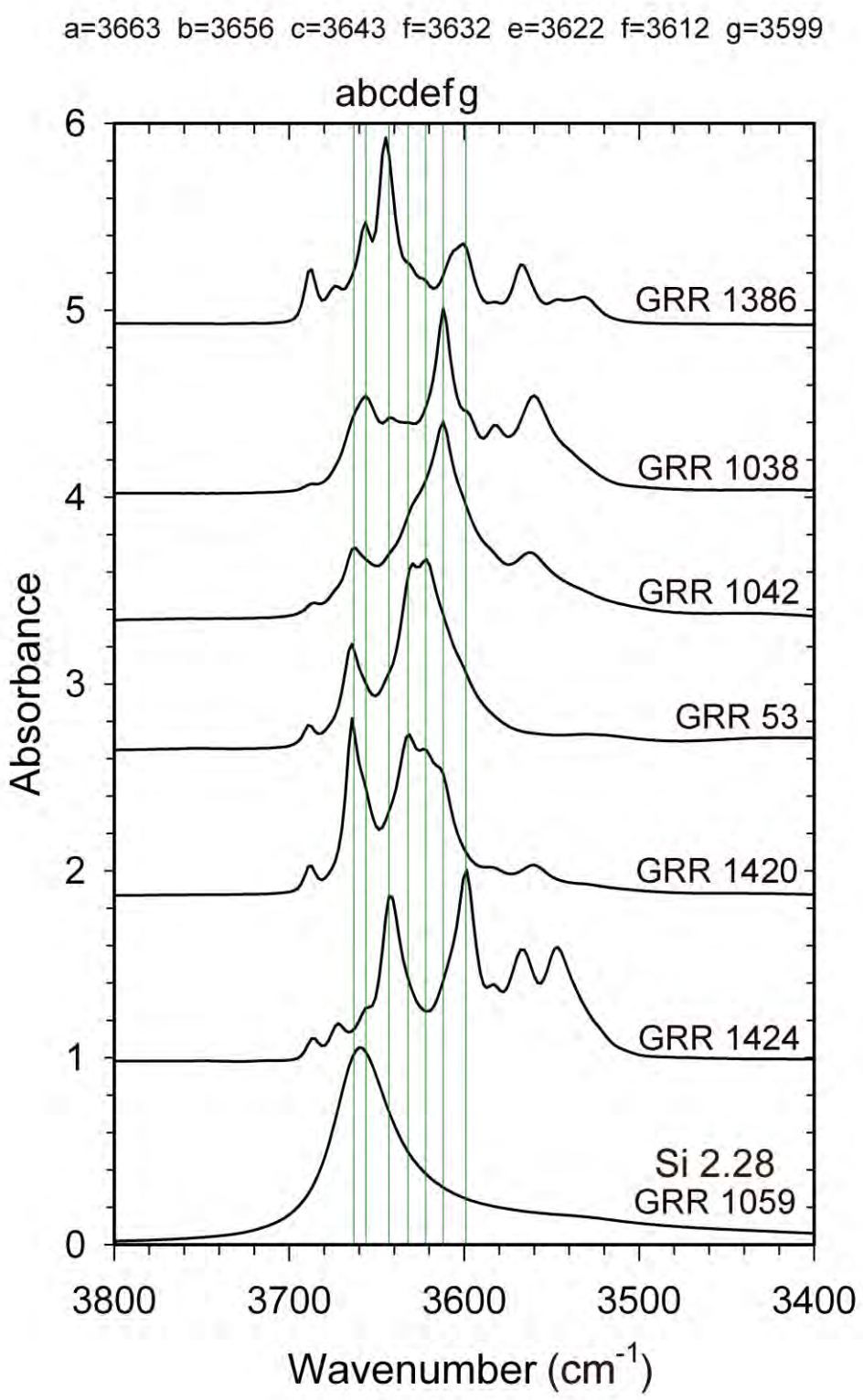

910

911

912 Figure 7.

913

914

This is a preprint, the final version is subject to change, of the American Mineralogist (MSA)
Cite as Authors (Year) Title. American Mineralogist, in press.
DOI: https://doi.org/10.2138/am-2020-7256

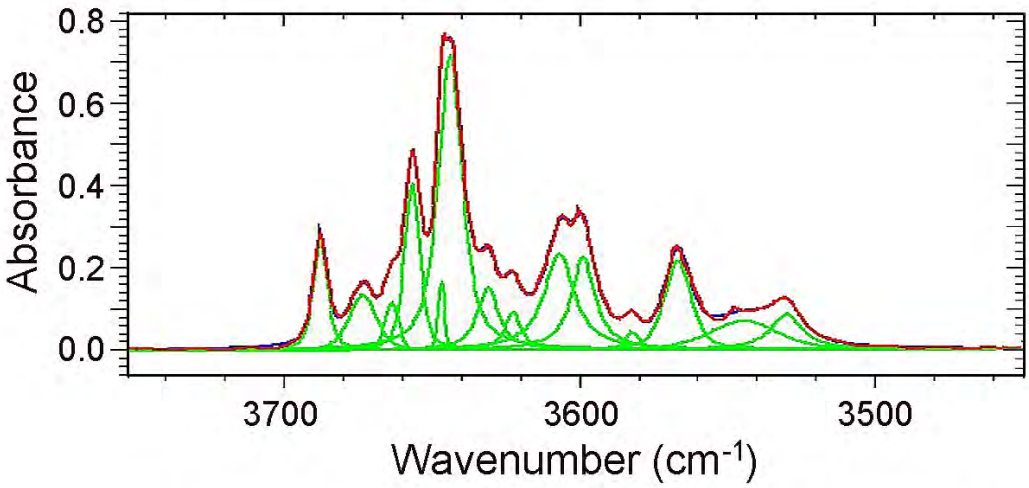

Curve Name	Centre	Width	Height	% Gaussian	Type	Area
Curve 1	3688	5.8	0.27	45	Mixed	2.08
Curve 2	3674	11.1	0.14	64	Mixed	1.86
Curve 3	3664	5.7	0.12	100	Mixed	0.71
Curve 4	3657	6.2	0.41	52	Mixed	3.34
Curve 5	3647	2.6	0.17	100	Mixed	0.47
Curve 6	3644	9.8	0.71	31	Mixed	9.98
Curve 7	3631	8.8	0.15	5	Mixed	2.07
Curve 8	3623	6.7	0.10	3	Mixed	0.96
Curve 9	3607	12.4	0.24	0	Mixed	4.63
Curve 10	3599	9.7	0.23	0	Mixed	3.47
Curve 11	3582	6.0	0.04	100	Mixed	0.27
Curve 12	3567	10.9	0.22	53	Mixed	3.10
Curve 13	3544	27.4	0.07	61	Mixed	2.45
Curve 14	3530	12.9	0.09	4	Mixed	1.74

915

916

917

918 Figure 8.

919

920

921

This is a preprint, the final version is subject to change, of the American Mineralogist (MSA)
Cite as Authors (Year) Title. American Mineralogist, in press.
DOI: https://doi.org/10.2138/am-2020-7256

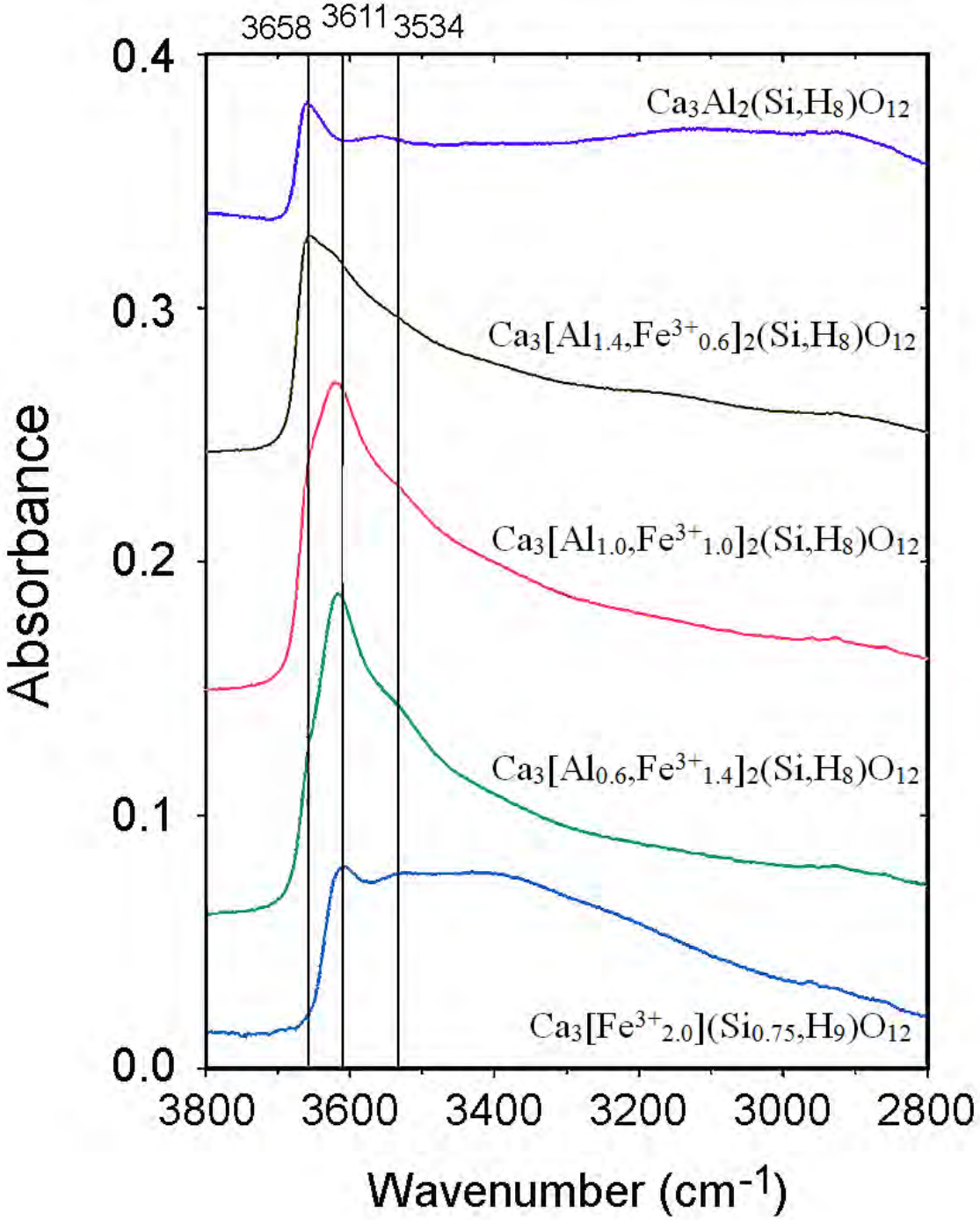

922

923

924

925 Figure 9.

926

927

928

929

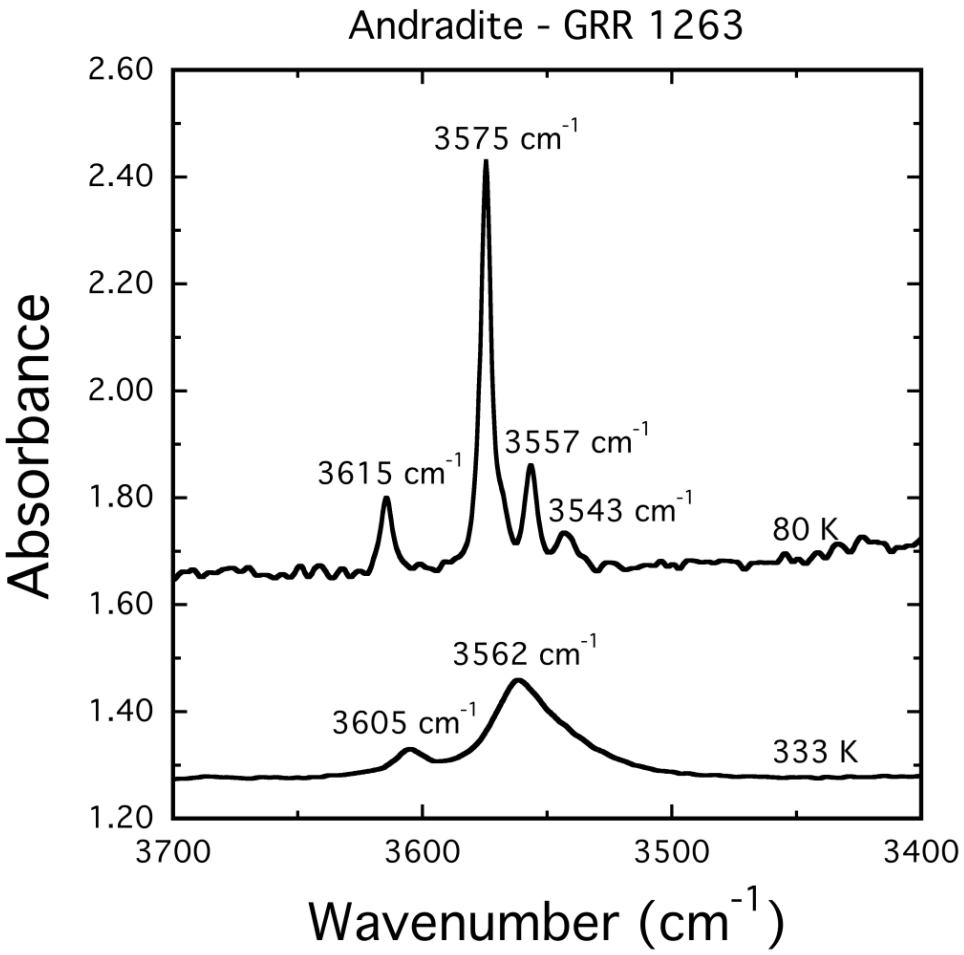

930

931

932

933

934 Figure 10.

935

936

937

938

This is a preprint, the final version is subject to change, of the American Mineralogist (MSA)
Cite as Authors (Year) Title. American Mineralogist, in press.
DOI: https://doi.org/10.2138/am-2020-7256

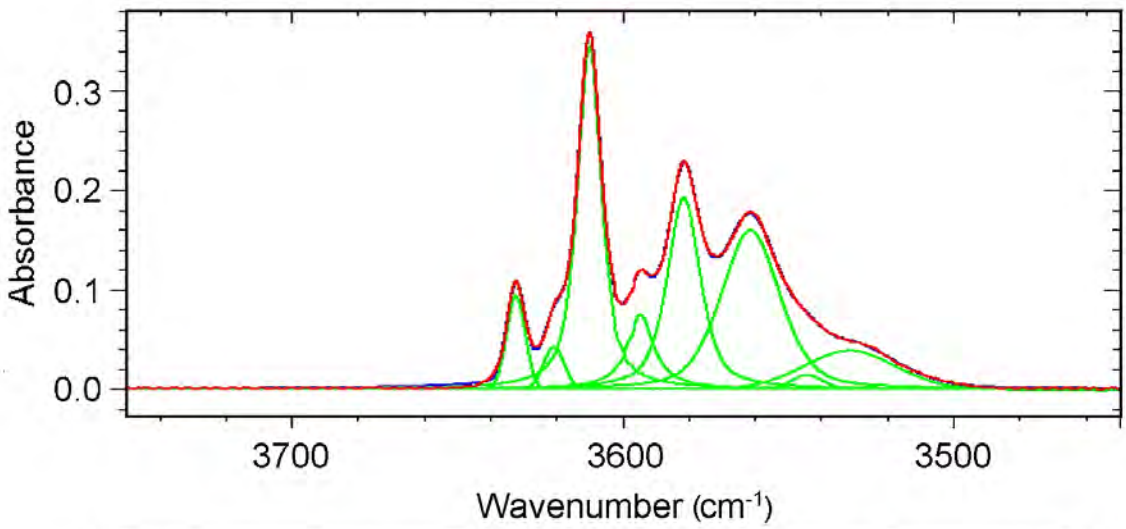

Curve Name	Centre	Width	Height	% Gaussian	Type	Area
Curve 1	3633	6.6	0.10	100	Mixed	0.67
Curve 2	3621	7.4	0.04	100	Mixed	0.34
Curve 3	3610	8.6	0.35	32	Mixed	4.22
Curve 4	3595	9.9	0.08	0	Mixed	1.17
Curve 5	3582	11.8	0.19	37	Mixed	3.17
Curve 6	3561	21.1	0.16	62	Mixed	4.26
Curve 7	3544	11.4	0.01	100	Mixed	0.18
Curve 8	3531	33.1	0.04	100	Mixed	1.38

Figure 11.

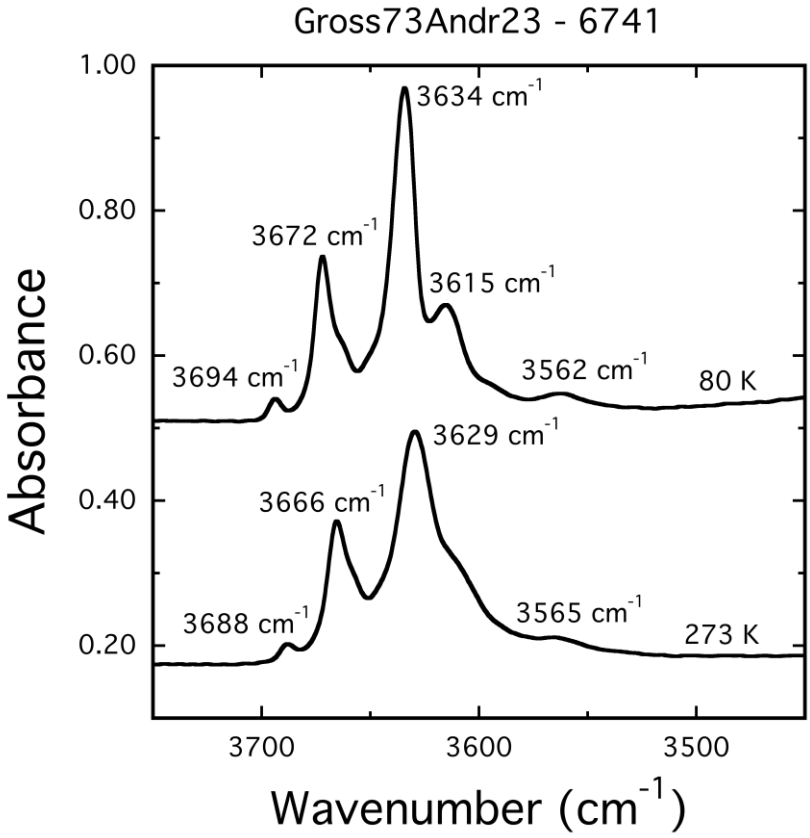

946 a.)

947

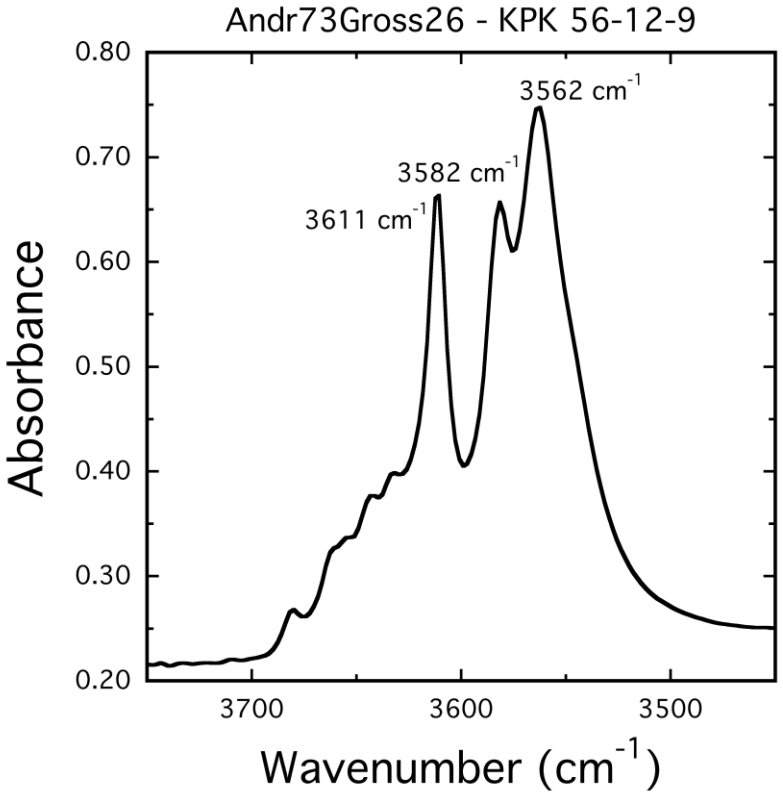

948 b.)

949 Figure 12.